MASTERARBEIT | MASTER'S THESIS

Titel | Title

Tikhonov Regularization in Photoacoustic Imaging

verfasst von | submitted by

Peter Školník BSc

angestrebter akademischer Grad | in partial fulfilment of the requirements for the degree of

Master of Science (MSc)

Wien | Vienna, 2026

Studienkennzahl lt. Studienblatt | Degree programme code as it appears on the student record sheet:	UA 066 821
Studienrichtung lt. Studienblatt | Degree programme as it appears on the student record sheet:	Masterstudium Mathematik
Betreut von | Supervisor:	Univ.-Prof. Dipl.-Ing. Dr. Otmar Scherzer

Abstract The aim of this thesis is to apply the theory of Tikhonov regularization to the problem of reconstructing the initial pressure in photoacoustic tomography. In the first chapter, we discuss the notion of an inverse problem due to Hadamard and what difficulties often arise when dealing with an inverse problem. We define the Moore-Penrose generalized inverse for a bounded, linear operator acting between Hilbert spaces and list its core properties. As a way to address the issue of instability, we review the basic regularization theory with a special focus on Tikhonov regularization. In the second chapter, we give a mathematical formulation of our problem - given the solution of the initial value problem for the wave equation on a part of the boundary of a bounded domain and for a finite time interval, we aim to reconstruct the initial value function inside this domain. We study under which conditions the initial value function is uniquely determined by the data. We present a uniqueness result first stated in [7], which we slightly adjusted to explicitly allow for finite measurement time. To apply the theory of Tikhonov regularization, we follow the work in [1] and formulate the problem in terms of a bounded, linear operator between two Hilbert spaces which describe the regularity of the involved functions. In the last chapter, we first describe the chosen numerical framework for the case of two line detectors. We numerically compare the method of solving a Tikhonov-regularized system of equations to an alternative method of time reversal. We study the case of sufficient measurement time as well as the one of shorter measurement times which do not satisfy the corresponding assumption of our uniqueness theorem. Herein, we resort to the k-Wave implementation of the forward initial value problem for the standard wave equation.

Abstract Das Ziel dieser Arbeit ist die Anwendung der Theorie der Tikhonov Regularisierung auf das Problem der Rekonstruktion des Anfangsdrucks in der photoakustischen Tomographie. Im ersten Kapitel führen wir den Begriff des inversen Problems nach Hadamard ein und studieren die Schwierigkeiten, die bei inversen Problemen häufig auftreten. Wir definieren die verallgemeinerte Moore-Penrose-Inverse für den Fall eines beschränkten linearen Operators zwischen zwei Hilberträumen und listen ihre grundlegenden Eigenschaften auf. Als Lösungsansatz für das Problem der Instabilität geben wir einen Überblick über die grundlegende Regularisierungstheorie mit besonderem Fokus auf die Tikhonov Regularisierung. Im zweiten Kapitel geben wir eine mathematische Formulierung unseres Problems: Wir verfügen über die Lösung des Anfangswertproblems für die Wellengleichung auf einer Teilmenge des Randes eines beschränkten Gebiets und in einem endlichen Zeitintervall und wir wollen die Anfangswertfunktion innerhalb dieses Gebiets rekonstruieren. Wir untersuchen, unter welchen Bedingungen die Anfangswertfunktion durch die Daten eindeutig bestimmt ist. Wir präsentieren ein Eindeutigkeitsresultat, das erstmals in [7] formuliert wurde und das wir leicht angepasst haben, um explizit endliche Messzeiten zuzulassen. Um die Theorie der Tikhonov Regularisierung anwenden zu können, folgen wir der Arbeit in [1] und formulieren das Problem mittels eines beschränkten linearen Operators zwischen zwei Hilberträumen, die die Regularität der in dem Problem auftretenden Funktionen beschreiben. Im letzten Kapitel beschreiben wir zuerst den gewählten numerischen Rahmen für den Fall zweier geradliniger Detektoren. Wir vergleichen numerisch unsere Methode, im Rahmen dessen wir ein Tikhonov-regularisiertes Gleichungssystem lösen, mit einer alternativen Methode der Zeitumkehr. Wir untersuchen sowohl den Fall einer hinreichenden Messzeit als auch den Fall kürzerer Messzeiten, die den Voraussetzungen unseres Eindeutigkeitsresultats nicht entsprechen. Zur Lösung des Anfangswertproblems verwenden wir die k-Wave Implementierung eines Lösungsverfahrens für die freie Wellengleichung.

Contents

1. Inverse Problems and Regularization Theory

1.1 Introduction to Inverse Problems

In this opening section, we would like to introduce gently the area of inverse problems and discuss their core properties.

Inverse problems, as a standalone area of mathematics, have been studied extensively for the last couple of decades. The main reason is their frequent appearance in many scientific fields, e.g. astronomy, geophysics or medical imaging. However, there is not only one school of thought regarding the definition of an inverse problem and in the end it is often application-specific. As the name suggests, an inverse problem should be in some sense inverse to another problem which could then be called direct. One does not need too much time to think of such a pair of problems. Arguably, the most straightforward one is integration and differentiation of a function $\mathbb{R} \to \mathbb{R}$. They are obviously inverse to each other in the sense that, given some function f, if one solves one of them first with the function f as input, takes the resulting output g and solves the other problem with g as input, what comes out of this will be (at least more or less, up to a constant) the function f one started with. However, this raises a question - since we just said one can basically go back and forth between the problems, should they not both be inverse (to each other)? Why is one called direct and the other inverse and how do we know which one is which? The traditional way to resolve this is to make use of Hadamard's definition of a "well-posed problem". According to [9], Hadamard called a problem well-posed if:

1. there is a solution to the problem
2. the solution is unique
3. the solution depends continuously on the data needed for its computation.

The first two conditions are there to ensure that we are not solving a problem with no solution or that there are multiple solutions and one needs to perform an additional selection. The third condition deals with the solvability of the problem in practice. After all, in reality we cannot expect to always have precise data at our disposal but rather have to assume that the data already comes with some degree of inaccuracy. The third condition imposed by Hadamard thus ensures that even if working with slightly inaccurate data, the computed solution will not deviate too much from the one computed with the perfect data. This property is called stability of the problem.

A problem which fails to satisfy at least one of these three items is called ill-posed. For our classification of direct/inverse, the (more) ill-posed one from the pair is then typically the inverse problem and the other one is the direct problem. Applying this to our example of integration and differentiation, we can impose conditions which would guarantee the existence and uniqueness of a solution for both. That leaves the third criterion to decide and in fact, integration tends to behave much more nicely regarding propagation of noise in the initial data than differentiation as the following example demonstrates.

Example 1 ([5])**.** Let $f, f^\delta \in C^2([0,1])$ be a function of interest together with its noisy version such that $\|f - f^\delta\|_\infty < \delta$. We first have a look at what happens if we integrate both. Using standard Riemann sums, we can find for an arbitrary $\varepsilon > 0$ a natural number $n \in \mathbb{N}$ such that

$$\left| \int_0^1 f(x)dx - \sum_{k=1}^{n} f(\frac{k}{n})\frac{1}{n} \right| < \varepsilon$$

and

$$\left| \int_0^1 f^\delta(x)dx - \sum_{k=1}^{n} f^\delta(\frac{k}{n})\frac{1}{n} \right| < \varepsilon.$$

Then we can easily see

$$\left| \int_0^1 f(x)dx - \sum_{k=1}^{n} f^\delta(\frac{k}{n})\frac{1}{n} \right| < \varepsilon + \delta$$

by the triangle inequality, thus the error stays quite well-behaved and in the same order of magnitude. Now let us have a look at what happens if we try to differentiate both functions using central finite differences. For a C^2-function, this scheme yields accuracy

$$\frac{f(x+h) - f(x-h)}{2h} = f'(x) + O(h).$$

Therefore,

$$\left| \frac{f^\delta(x+h) - f^\delta(x-h)}{2h} - f'(x) \right| < O(h) + \frac{\delta}{h}.$$

In this case we see a completely different type of behavior. The extra error term which comes from using the noisy data does not stay bounded and in fact grows as one refines the discretization. Using an arbitrary constant $C > 0$ to express the right hand side as $Ch + \frac{\delta}{h}$, it is a simple exercise to find the global minimum for $h > 0$ at $h_0 = \sqrt{\frac{\delta}{C}}$. This shows that there is an optimal discretization level beyond which the data error takes over and the total error starts increasing again. This hints at the need for compromising between accuracy in the case of perfect data and stability in the case of noisy data. We will revisit this idea in more detail in later sections.

Therefore, we would refer in this case to integration and differentiation as the direct and the inverse problem, respectively. When considering problems from a mathematical or numerical perspective, Hadamard's definition of well-posedness is the tool of choice in the classification of inverse problems.

Nonetheless, when considering a problem from the perspective of its real-world application, one sometimes uses the alternative characterization that "an inverse problem is such where one is concerned with determining from observations the causalities which caused them". A nice example of that is recovering an object's image from x-ray measurements in computed tomography. These two characterizations often coincide but may also differ.

Curiously enough, back in his time, Hadamard did not believe that real-world problems can be ill-posed. Nowadays, we know that they indeed can.

1.2 General Treatment of Inverse Problems

In this section, we define the notion of a least-squares solution and Moore-Penrose inverse and list their basic properties. We closely follow the exposition in [5].

After a brief discussion of what inverse problems are, we would like to talk about how to solve them. In everything that follows, we will consider linear equations of the type

$$Ax = y \tag{1}$$

where $A : X \to Y$ is a bounded, linear operator between two Hilbert spaces $(X, \|\cdot\|_X)$ and $(Y, \|\cdot\|_Y)$. Looking again at Hadamard's well-posedness law, we can translate violations of the three conditions as:

1. The vector y is not in the range of A (this means that A is not surjective).

2. There is more than one vector x which satisfies the equation (this means that A is not injective).

3. The inverse operator A^{-1} is not continuous.

The first two items mean that the inverse A^{-1} is not well-defined. The way to tackle this issue is to introduce a new notion of a solution.

Definition 1. Let $A : X \to Y$ be as above and $y \in Y$. We call $x^* \in X$ a **least-squares solution** of Equation 1 if

$$||Ax^* - y||_Y = \inf_{x \in X} ||Ax - y||_Y.$$

Moreover, $x^* \in X$ is called a **best-approximate solution** if it is a least-squares solution and

$$||x^*||_X = \inf\left\{||x||_X : x \in X \text{ is a least squares solution of Equation 1}\right\}.$$

The minimal norm condition on one hand fulfills the role of a criterion in case we need to choose from different solutions (however, at this point, it is not clear that this ensures uniqueness). On the other hand, from a practical point of view, it also has a smoothing role - imposing the smallest norm possible often ensures that the solution is better-behaved. For example, when looking for weak solutions of differential equations, we may choose the L^2 or H^1 norm as the norm $||\cdot||_X$. Then, imposing such a condition on the norm of the solution often avoids oscillatory behavior or blow-up in the solution.

We would like to define an operator which maps to best-approximate solutions. To this end, let's first consider the operator

$$\hat{A} : ker(A)^\perp \to ran(A)$$

$$\hat{A}x := A\Big|_{ker(A)^\perp} x.$$

This operator is injective since $ker(A)^\perp$ is a subspace of X and for $x_1, x_2 \in ker(A)^\perp$ it holds

$$Ax_1 = Ax_2 \implies x_1 - x_2 \in ker(A) \cap ker(A)^\perp \implies x_1 - x_2 = 0.$$

It is also surjective since, by definition, we can for any $y \in ran(A)$ find an $x \in X$ with $Ax = y$ and this (just as any) x can be written as $x = x_1 + x_2$ with $x_1 \in ker(A)$ and $x_2 \in ker(A)^\perp$. Therefore, $\hat{A}$ possesses an inverse $\hat{A}^{-1}$. We note that this inverse already fulfills what we want if $y \in ran(A)$. Namely, in that case the inverse yields the unique solution orthogonal to $ker(A)$ which is therefore the one of minimal norm according to the Pythagorean theorem. To be able to consider a wider class of equations, we can now enlarge the domain of our new operator to $ran(A) \bigoplus ran(A)^{\perp}$. In fact, any $y \in ran(A) \bigoplus ran(A)^{\perp}$ can be, by definition, written uniquely as $y_1 + y_2$ with $y_1 \in ran(A)$ and $y_2 \in ran(A)^{\perp}$. Then, we can see by using the Pythagorean theorem again that the least squares condition decomposes into

$$||Ax - y||_Y^2 = ||Ax - y_1||_Y^2 + ||y_2||_Y^2.$$

This means on one hand that we cannot do better than $||y_2||_Y^2$, but on the other hand also that we can do precisely $||y_2||_Y^2$. In fact, the first summand is equal to zero for $x = \hat{A}^{-1} y_1$. Moreover, as we already argued, this x has minimal norm. We summarize our construction in the following definition.

Definition 2. Let $A : X \to Y$ be a bounded, linear operator. Then, using the operator $\hat{A}^{-1}$ defined above, **Moore-Penrose generalized inverse** is defined as

$$\begin{aligned} A^{\dagger} : D(A^{\dagger}) &\to ker(A)^{\perp} \\ y_1 + y_2 &\mapsto \hat{A}^{-1} y_1 \end{aligned}$$

where $D(A^{\dagger}) := ran(A) \bigoplus ran(A)^{\perp}$ and so $y_1 + y_2 \in D(A^{\dagger})$ is already in the decomposed form.

In the following theorem, we collect the most important properties of the Moore-Penrose inverse.

Theorem 1 ([5])**.** Let $A : X \to Y$ be a bounded, linear operator and let $A^{\dagger}$ be its Moore-Penrose inverse. The following items hold:

1. for $y \in D(A^{\dagger})$, $x^{\dagger} := A^{\dagger} y$ is the unique best-approximate solution of $Ax = y$;

2. $A^{\dagger}$ is bounded if and only if $ran(A)$ is closed;

3. for $y \in D(A^{\dagger})$, $x^* \in X$ is a least-squares solution of Equation 1 if and only if $A^* A x^* = A^* y$ where $A^* : Y \to X$ is the adjoint operator of A. This is called the normal equation.

The Moore-Penrose inverse is our remedy for the issues of non-injectivity and non-surjectivity. However, the last item in Hadamard's law, the stability, still remains uncovered. The second item in the last theorem tells us that $A^{\dagger}$ can be bounded if and only if $ran(A)$ is closed. Unfortunately, for a significant class of operators this almost never happens.

Corollary 1 ([5])**.** Let $K : X \to Y$ be a compact, linear operator such that $ran(K)$ is infinite-dimensional. Then $K^\dagger$ is not bounded.

Proof. Let us suppose $K^\dagger$ is in fact bounded (and therefore continuous). The operator $K^\dagger$ is an extension of the bijective operator $\hat{K}$ ($\hat{K}$ is defined just as $\hat{A}$ was before for the case of a bounded, linear operator) and by elementary functional analysis $\hat{K}$ is continuously invertible. By Theorem 1, $ran(K)$ is closed. Since a composition of a bounded and a compact operator is again compact, this would imply that the operator $K\hat{K}^{-1} : ran(K) \to ran(K)$ is compact. However, $K\hat{K}^{-1}$ is the identity operator on $ran(K)$ and as such can only be compact if $ran(K)$ is finite-dimensional. ■

In particular, we note that integral operators, which appear frequently in various applications, are often compact and therefore their generalized inverse is definitely not continuous. After all, we saw an indication of this fact already in Example 1 with integration and differentiation in the previous section. We tackle this issue in depth in the next section. But, before that, we would like to offer one more perspective on why in the case of a compact, linear operator one should expect noise amplification and consequently an error in the computed solution if the data is noisy.

To this end, consider a compact, self-adjoint operator $K : X \to X$. By the famous spectral theorem for compact, self-adjoint operators, there is a monotonically decreasing sequence of eigenvalues $\lambda_n \to 0$ with $\lambda_n \neq 0$ and a sequence of corresponding orthonormal eigenvectors v_n of K spanning $ker(K)^\perp$ such that every $x \in X$ can be written as

$$x = \sum_n \langle v_n, x \rangle v_n \; + \; h$$

with a unique $h \in ker(K)$. This implies

$$Kx = \sum_n \lambda_n \langle v_n, x \rangle v_n$$

and allows for a similar representation of $K^\dagger$. Namely, for $y = y_1 + y_2 \in ran(K) \bigoplus ran(K)^\perp$ we have $\langle v_n, y \rangle = \langle v_n, y_1 \rangle$ because $v_n \in ran(K)$ for all n. Therefore,

$$y_1 = \sum_n \langle v_n, y \rangle v_n = \sum_n \langle v_n, Kx \rangle v_n$$

for a unique $x \in ker(K)^\perp$. Now,

$$\langle v_n, Kx \rangle = \langle K v_n, x \rangle = \lambda_n \langle v_n, x \rangle$$

leads us to the representation

$$x^\dagger = \sum_n \frac{\langle v_n, y\rangle}{\lambda_n} v_n$$

since $\lambda_n \neq 0$. If we do not know the exact data y but only its approximation y^δ with $\|y - y^\delta\| \leqslant \delta$, we can see using the Cauchy-Schwarz inequality that the error we make in the inner products is roughly of the same order

$$\left|\langle v_n, y\rangle - \langle v_n, y^\delta\rangle\right| = \left|\langle v_n, y - y^\delta\rangle\right| \leqslant \|v_n\|\|y - y^\delta\| \leqslant \delta.$$

This means that in the infinite sum, the error in the numerator gets amplified by the smaller and smaller denominators (to such an extent that the operator becomes discontinuous).

Last but not least, we note that this representation also offers one possible way out - truncating the infinite sum at some n and stopping the noise amplification. This is known as singular value truncation (since this can be more generally carried out for compact operators using their singular value decomposition) and is, in fact, one of the possible solutions to the issue. Another option is to alter the eigenvalues such that their reciprocals do not converge to infinity anymore. One way to do this is to shift the pole slightly away from zero and consider instead $\frac{1}{\lambda_n + \alpha}$ for some $\alpha > 0$. The approximate solution x_α^δ of Equation 1 with noisy data y^δ would then be

$$x_\alpha^\delta = \sum_n \frac{\langle v_n, y^\delta\rangle}{\lambda_n + \alpha} v_n.$$

We will see that this is indeed a way to solve the instability problem.

1.3 Introduction to Regularization Theory

In this section, we would like to lay the theoretical grounds for a rigorous treatment of the case when the Moore-Penrose inverse is unbounded. Therefore, we first define the notion of a regularization for the Moore-Penrose inverse and then present a couple of theorems suggesting how to easily obtain these regularizations. As in the previous section, we follow the approach in [5].

The basic idea of regularization is to construct a continuous approximation of the operator $A^\dagger$ and apply it to the noisy data y^δ, hoping this will result in a more stable process and a better approximation of $A^\dagger y$ than $A^\dagger y^\delta$. We note that the latter may not even exist since in the considered case $ran(A)$ is not closed and so $D(A^\dagger)$ is a proper subset of Y.

We can even increase our requirements and require that there is a series of approximating continuous operators, let us call them A_α, producing a series of approximating solutions x_α^δ such that, for the noise level $\delta \to 0$ and $\alpha \to 0$ simultaneously, we would get $x_\alpha^\delta \to x^\dagger$. The parameter α will describe the degree of regularization and we will call it the regularization parameter. In practice, it often describes the compromise between accuracy and stability. The higher the parameter is, the more stable the operator A_α is (one can think of it as the operator norm decreasing with increasing α). This comes however at the cost of lower accuracy when comparing $A^\dagger y$ and $A_\alpha y$ (one could say the operator A_α less and less "resembles" the original reconstruction operator $A^\dagger$). While only a heuristic, it often proves useful. This leads us to the following definition.

Definition 3. Let $A : X \to Y$ be a bounded, linear operator and $\alpha_0 > 0$. We call a family of continuous linear operators $A_\alpha : Y \to X$ with $\alpha \in (0, \alpha_0)$ **a regularization for** $A^\dagger$ if there is for every $y \in D(A^\dagger)$ a parameter choice function $\alpha : \mathbb{R}^+ \times Y \to (0, \alpha_0)$ such that both

$$\lim_{\delta \to 0} \sup \left\{ \|A_{\alpha(\delta, y^\delta)} y^\delta - A^\dagger y^\delta\| \ : \ y^\delta \in Y, \|y^\delta - y\| \leqslant \delta \right\} = 0$$

and

$$\lim_{\delta \to 0} \sup \left\{ \alpha(\delta, y^\delta) \ : \ y^\delta \in Y, \|y^\delta - y\| \leqslant \delta \right\} = 0$$

hold.

Thus, even though we aim to regularize the general reconstruction operator $A^\dagger$, the parameter choice function can be different for every right-hand side. Probably the first question which arises is how to construct such a family of regularizing operators. The next theorem presents one possibility.

Theorem 2 ([5])**.** If a sequence of continuous linear operators $A_\alpha : Y \to X$ satisfies $A_\alpha y \to A^\dagger y$ for $\alpha \to 0$ and any $y \in D(A^\dagger)$, then it is a regularization for $A^\dagger$ and for every $y \in D(A^\dagger)$ there is an a priori parameter choice function (meaning it only depends on the noise level δ).

Thus, families of continuous operators which converge pointwise to the Moore-Penrose inverse do the trick. To find suitable families of this nature, we make use of the fact that the best-approximate solution is described by the normal equation

$$A^* A x = A^* y.$$

We can therefore work with the operator $A^*A : X \to X$ instead of A which has the advantage that this operator is clearly self-adjoint. At this point, it is also useful to refresh the observations from the previous section: using the eigenvalue decomposition for a compact, self-adjoint operator, one could see the source of instability as well as one potential way of regularizing the solution operator. If the operator is only bounded and self-adjoint, we can resort to the spectral theorem for bounded, self-adjoint operators and essentially replace the eigenvalue decomposition with the spectral representation. More concretely, let us consider a general bounded, self-adjoint operator $T : X \to X$. Denoting the standard Borel sigma algebra on $\mathbb{R}$ by $\mathscr{B}(\mathbb{R})$ and the space of all bounded, linear operators $X \to X$ by $L(X)$, it holds by the spectral theorem for bounded, self-adjoint operators that there exists a unique spectral measure $E : \mathscr{B}(\mathbb{R}) \to L(X)$ with compact support on $\mathbb{R}$ such that

$$T = \int_{\mathbb{R}} \lambda \, dE_\lambda.$$

Moreover, this famously defines a functional calculus of T in the sense that if $f : \mathbb{R} \to \mathbb{R}$ is a bounded, Borel-measurable function, then

$$f(T) := \int_{\mathbb{R}} f(\lambda) \, dE_\lambda$$

defines a bounded operator. This construction has, among others, the property that for $f, g : \mathbb{R} \to \mathbb{R}$ bounded, Borel-measurable it holds $(f \cdot g)(T) = f(T) \cdot g(T)$. In particular, this implies that if $0 \notin \sigma(T)$, the inverse of T is simply given as

$$T^{-1} = \int_{\mathbb{R}} \frac{1}{\lambda} \, dE_\lambda.$$

However, in general, the inverse is not well-defined. This translates into 0 being in the spectrum which makes the integral not defined since $\frac{1}{\lambda}$ is then not a bounded, Borel-measurable function on the spectrum of T. Nonetheless, this representation is a good source of regularizations as we defined them. Namely, one could try to replace $\frac{1}{\lambda}$ with a sequence of functions $g_\alpha(\lambda)$ such that they are on one hand pointwise converging to $\frac{1}{\lambda}$ for $\alpha \to 0$ but on the other hand also continuous over the whole spectrum and thus definitely integrable. The next theorem embodies these ideas.

Theorem 3 ([5])**.** Let $A : X \to Y$ be a bounded, linear operator and $\alpha_0 > 0$. Let $g_\alpha : [0, \|A\|^2] \to \mathbb{R}$, $\alpha \in (0, \alpha_0)$ be a sequence of functions such that the following conditions are satisfied:

1. g_α is piecewise continuous for all $\alpha \in (0,\alpha_0)$;
2. There is a constant $C > 0$ such that $|\lambda g_\alpha(\lambda)| \leqslant C$ for all $\alpha \in (0,\alpha_0)$ (C is independent of α);
3. $\lim_{\alpha\to 0} g_\alpha(\lambda) = \frac{1}{\lambda}$ for all $\lambda \in (0, \|A\|^2]$

Then we have for all $y \in D(A^\dagger)$ the convergence

$$\lim_{\alpha\to 0} g_\alpha(A^*A)A^*y = x^\dagger.$$

In particular, $g_\alpha(A^*A)A^*$ is a regularization for $A^\dagger$ by Theorem 2.

1.4 Tikhonov Regularization

In this section, we describe a special case of Theorem 3 - the Tikhonov regularization.

We return now to our idea from the end of Section 1.2. There we proposed replacing $\frac{1}{\lambda_n}$ in the orthonormal expansion of $x^\dagger$ with $\frac{1}{\lambda_n+\alpha}$ in the case of a compact, self-adjoint operator. In light of Theorem 3, this corresponds to setting $g_\alpha(\lambda) := \frac{1}{\lambda+\alpha}$ for the bounded, self-adjoint operator A^*A. Since the functions g_α satisfy the assumptions of this theorem, this yields the regularization

$$g_\alpha(A^*A) = \int_{\mathbb{R}} \frac{1}{\lambda+\alpha}\, dE_\lambda = (A^*A+\alpha I)^{-1}$$

of A^*A. This is called **Tikhonov regularization**. This regularization is closely related to the so-called **Tikhonov functional** $X \to [0,\infty)$ defined for an operator $A : X \to Y$ and $y \in Y$ via

$$x \mapsto \|Ax-y\|_Y^2 + \alpha\|x\|_X^2.$$

The next theorem explains this relation.

Theorem 4 ([5]). Let $A : X \to Y$ be a bounded, linear operator and $x_\alpha := (A^*A+\alpha I)^{-1}A^*y$ for $\alpha > 0$ and $y \in Y$. Then x_α is the unique minimizer of the Tikhonov functional defined above.

Proof. For $\alpha > 0$ and $y \in Y$, we set $F_\alpha(x) := \|Ax-y\|_Y^2 + \alpha\|x\|_X^2$ for the Tikhonov functional and observe that it is strictly convex. In fact, taking arbitrary $x_1,x_2 \in X$ and $\gamma \in (0,1)$ such that $x_1 \neq x_2$ we need to show

$$F_\alpha\big(\gamma x_1 + (1-\gamma)x_2\big) < \gamma F_\alpha(x_1) + (1-\gamma)F_\alpha(x_2)$$

or equivalently

$$\gamma F_\alpha(x_1) + (1-\gamma)F_\alpha(x_2) - F_\alpha\big(\gamma x_1 + (1-\gamma)x_2\big) > 0. \tag{2}$$

We start by expanding

$$\begin{aligned}
F_\alpha\big(\gamma x_1 + (1-\gamma)x_2\big) &= \big\|A(\gamma x_1 + (1-\gamma)x_2) - y\big\|_Y^2 + \alpha\big\|\gamma x_1 + (1-\gamma)x_2\big\|_X^2 \\
&= \gamma^2\|Ax_1 - y\|_Y^2 + (1-\gamma)^2\|Ax_2 - y\|_Y^2 \\
&\quad + 2\gamma(1-\gamma)\big\langle Ax_1 - y, Ax_2 - y\big\rangle_Y \\
&\quad + \alpha\gamma^2\|x_1\|_X^2 + \alpha(1-\gamma)^2\|x_2\|_X^2 \\
&\quad + 2\alpha\gamma(1-\gamma)\big\langle x_1, x_2\big\rangle_X.
\end{aligned}$$

Adding and subtracting $\gamma F_\alpha(x_1) + (1-\gamma)F_\alpha(x_2)$ in the last expression enables us to write the difference in Inequality 2 as

$$\begin{aligned}
&\gamma(1-\gamma)\left[\|Ax_1 - y\|_Y^2 - 2\langle Ax_1 - y, Ax_2 - y\rangle_Y + \|Ax_2 - y\|_Y^2\right] \\
&+ \gamma(1-\gamma)\alpha\left[\|x_1\|_X^2 - 2\langle x_1, x_2\rangle_X + \|x_2\|_X^2\right]
\end{aligned}$$

or

$$\gamma(1-\gamma)\big\|(Ax_1 - y) - (Ax_2 - y)\big\|_Y^2 + \gamma(1-\gamma)\alpha\big\|x_1 - x_2\big\|_X^2$$

which is clearly positive since $x_1 \neq x_2$. We also have

$$\lim_{\|x\|\to\infty} F_\alpha(x) = \infty$$

and so the functional has a unique minimum x^* characterized by the condition

$$F_\alpha'(x^*)h = 0 \text{ for all } h \in X.$$

This finishes the proof since

$$\begin{aligned}
F_\alpha'(x)h = \frac{d}{dt}\Big|_{t=0} F_\alpha(x + th) &= 2\big(\langle Ah, Ax - y\rangle_Y + \alpha\langle x, h\rangle_X\big) \\
&= 2\big\langle h, (A^*A + \alpha I_X)x - A^*y\big\rangle.
\end{aligned}$$

■

Thus, Theorem 4 tells us that applying the Tikhonov regularization is equivalent to solving the least-squares equation enriched by an additional term controlling the norm of the solution.

From Theorem 3, it follows that for $y \in D(A^\dagger)$ we have the convergence $x_\alpha \to A^\dagger y$ with $x_\alpha := (A^*A + \alpha I)^{-1}A^*y$. However, we are, of course, much more interested in what happens if we use the noisy version y^δ of y. We set $x_\alpha^\delta := (A^*A + \alpha I)^{-1}A^*y^\delta$ and want to see whether also $x_\alpha^\delta \to A^\dagger y$ for $\alpha, \delta \to 0$ simultaneously. Since there are now two different parameters α and δ, we are looking for a suitable parameter choice function such that the convergence holds. To this end, we follow [8] and start by splitting the error

$$\|x_\alpha^\delta - A^\dagger y\|_X \leqslant \|x_\alpha^\delta - x_\alpha\|_X + \|x_\alpha - A^\dagger y\|_X.$$

We already know about the convergence of the second term. For the first one, we use (here we emphasize with a subscript in which underlying space the identity operator is defined to avoid confusion)

$$(A^*A + \alpha I_X)^{-1}A^* = A^*(AA^* + \alpha I_Y)^{-1}$$

to write

$$\begin{aligned}
\|x_\alpha^\delta - x_\alpha\|_X^2 &= \|A^*(AA^* + \alpha I_Y)^{-1}(y^\delta - y)\|_X^2 \\
&= \left\langle A^*(AA^* + \alpha I_Y)^{-1}(y^\delta - y), A^*(AA^* + \alpha I_Y)^{-1}(y^\delta - y)\right\rangle_X \\
&= \left\langle (AA^* + \alpha I_Y)^{-1}(y^\delta - y), AA^*(AA^* + \alpha I_Y)^{-1}(y^\delta - y)\right\rangle_Y \\
&\leqslant \|(AA^* + \alpha I_Y)^{-1}(y^\delta - y)\|_Y \|AA^*(AA^* + \alpha I_Y)^{-1}(y^\delta - y)\|_Y \\
&\leqslant \frac{\delta}{\alpha} \cdot \delta
\end{aligned}$$

which implies

$$\|x_\alpha^\delta - x_\alpha\|_X \leqslant \frac{\delta}{\sqrt{\alpha}}\,.$$

This leaves us with the final estimate

$$\|x_\alpha^\delta - A^\dagger y\|_X \leqslant \frac{\delta}{\sqrt{\alpha}} + \|x_\alpha - A^\dagger y\|_X. \tag{3}$$

At this point, we recognize the phenomenon already encountered in the opening section. Namely, our error consists of two terms representing the regularization error in the case of perfect data and the error caused by using noisy data with the regularization level fixed, respectively. We also see, similarly to the example with differentiation, that for a given noise level we must not simply choose α as small as possible because the data error term would explode. Instead, there is an optimal regularization parameter minimizing the sum of the two error terms. Nonetheless, for a varying noise level we get:

Theorem 5 ([5]). Let $y \in ran(A)$, $\delta > 0$ and $y^\delta \in D(A^\dagger)$ with $\|y - y^\delta\| \leqslant \delta$. With x_α^δ defined as above, we get for any a priori parameter choice function $a : [0,\infty) \to (0,\infty)$ satisfying $\lim_{\delta\to 0} a(\delta) = 0$ and $\lim_{\delta\to 0} \frac{\delta}{\sqrt{a(\delta)}} = 0$ the convergence

$$\lim_{\delta\to 0} x_{a(\delta)}^\delta = A^\dagger y.$$

2. Photoacoustic Tomography

2.1 Photophone and Photoacoustic Effect

In this section, we aim to give a little background behind the discovery of the photoacoustic effect which is central to today's photoacoustic tomography.

Alexander Graham Bell's invention of the telephone in 1876 is without any doubt one of the greatest inventions of mankind. It revolutionized worldwide communication in ways not previously thought of. Therefore, for almost anyone it would be surprising to hear that Bell did not consider the telephone his greatest invention. When he said the words "This is the greatest invention I have ever made, even greater than the telephone." shortly before his death, he was talking about his 1880 invention of the photophone.

As Bell describes in his work [2], in the late 1870s he and his colleague Sumner Tainter conducted a series of experiments trying to create a wireless communication device. They were especially interested in the fact that the electrical resistance of selenium varies significantly with the amount of light it is exposed to. After numerous trials, they came up with the following idea to use this property to their advantage. They arranged a plane mirror made of a sufficiently flexible material such as microscope glass and a beam of light shining directly onto it. As Tainter was speaking towards the backside of the mirror, due to the air pressure the mirror was turning alternately convex and concave. These changes resulted in a reflection of the light with varying intensity. The reflected light would then fall onto a thin selenium cell connected to a local circuit with a battery and a telephone. Depending on the varying light, the momentary electrical resistance of the selenium cell would vary, too.

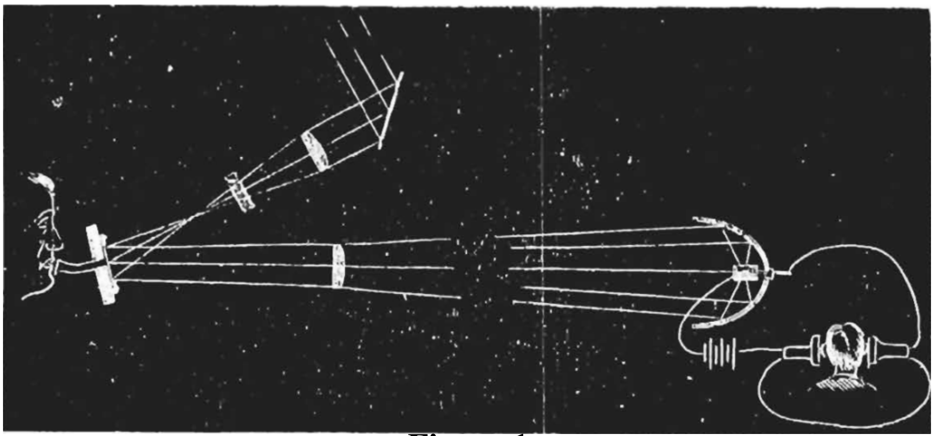

Figure 1
Scheme of Bell's and Tainter's experiment from [2]

This would in turn alter the electrical signal coming from the battery which would then reach the telephone at Bell's ear. As Bell notes, Tainter would stand on the roof of the Franklin School House in Washington while Bell was inside his office across the street. Despite the distance between them being over 200 meters, Bell states that he could hear the words "Mr. Bell, if you hear what I say, come to the window and wave your hat." as clearly as ever. We refer to Figure 1 for a scheme of their setup.

Even more interestingly, in subsequent experiments the two removed the battery and the telephone completely. Bell would simply put a thin layer of the used material (they tried many different ones) to his ear and let the reflected light shine onto it. Depending on the material, the intensity of the speech or musical tones would vary but even with a paper layer, Bell would hear at least some indistinct sounds. Their finding was later described more thoroughly and named the photoacoustic effect. This refers to the ability of materials to absorb light energy coming with varying intensity and produce heat. The produced heat in turn results in alternating expansion and contraction of the material based on the varying temperature. This creates the measured acoustic pressure.

2.2 Introduction to Photoacoustic Tomography

In this section, we give a mathematical formulation of the central problem in photoacoustic tomography and establish a couple of similarities to computed tomography.

The photoacoustic effect described in the previous section is the core of today's photoacoustic tomography (PAT). PAT combines the high contrast of optical imaging with the spatial resolution of ultrasound, making it a promising modality for applications ranging from breast cancer detection to vascular imaging. One typical setup for PAT is described in [13] and goes as follows: a

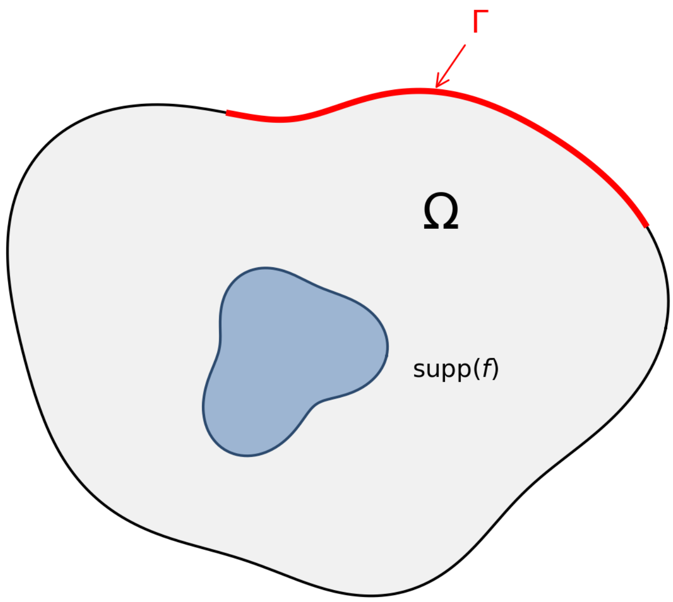

Figure 2
The geometry of the photoacoustic problem in $\mathbb{R}^2$

laser emits short laser pulses hitting the object of interest which, undergoing thermal expansion caused by the photoacoustic effect, creates an acoustic pressure measured by transducers positioned nearby. The collection of transducers can form a line, a plane, a sphere or have different geometric properties. This process is typically repeated numerous times while the transducers change their position to gather data from many different angles. One then hopes that, given a sufficient amount of data (both from enough positions and measured for a long enough time), it is possible to reconstruct the initial pressure distribution of the object. A good example to demonstrate this is the diagnosis of breast cancer. It is well-known that cancerous cells react differently to such a laser pulse than healthy cells. Namely, they emit more heat and expand more, thereby creating a different acoustic pressure. If we knew the initial pressure distribution inside the object, we would know which cells might be damaged.

Since the problem can be in principle considered in an arbitrary space $\mathbb{R}^n$ and we later carry out our numerical experiments in the two-dimensional setting, we will consider $\mathbb{R}^n$ with $n = 2,3$. Mathematically, we may express this problem as follows. We start off with a bounded set $\Omega \subseteq \mathbb{R}^n$. The so-called observation surface $\Gamma \subseteq \partial\Omega$ describes the position of our transducers and the final observation time is denoted by $T > 0$. Our task is then to reconstruct the compactly supported initial pressure function $f(x)$ with $x \in \text{supp}(f) \subseteq \Omega$ from the acoustic pressure $g(\sigma,t)$ with $\sigma \in \Gamma$ and $t \in [0,T]$. For clarity, the corresponding situation in $\mathbb{R}^2$ is shown in Figure 2. Since what is measured are acoustic waves, one model is that the propagation of photoacoustic wave pressure is governed by the wave equation and thus satisfies

$$\begin{cases} p_{tt} - c^2 \Delta p = 0 \text{ in } \mathbb{R}^n \times (0,\infty) \\ p(x,0) = f(x) \text{ in } \Omega \\ p(x,0) = 0 \text{ in } \mathbb{R}^n \setminus \Omega \\ p_t(x,0) = 0 \text{ in } \mathbb{R}^n \end{cases} \tag{4}$$

where p_{tt} denotes the second partial derivative of p with respect to time, Δp is the spatial Laplacian of p and $c : \mathbb{R}^n \to \mathbb{R}$ is the speed of sound. Although, as indicated, the speed of sound is usually spatially varying, we will assume in our theoretical considerations that it is equal to a constant. Furthermore, this constant can be taken equal to one since otherwise we can simply scale the solution accordingly. Our data g then satisfies

$$p(\sigma,t) = g(\sigma,t) \text{ on } \Gamma \times [0,T].$$

Keeping in mind our opening section on inverse problems, what naturally follows after formulating the problem is the question of well-posedness. Already the first question, the question of existence of a solution, is a non-trivial one. Later, we will introduce the so-called photoacoustic operator mapping initial pressure to the measurements on the observation surface. The question of existence is equivalent to characterizing the range of the operator. This has been done in special cases of observation surfaces, e.g. for a sphere. In the following, we will simply assume there is a solution. The next question is the question of uniqueness: given the acoustic pressure measured on the observation surface, is there only one initial pressure function giving rise to it? From a practical point of view, this is a very important question since if the answer is no, we cannot be sure that the patient's diagnosis we came up with is the correct one. We will see in the next section that, under suitable assumptions (which are in general not too hard to satisfy), we have indeed guaranteed uniqueness of reconstruction. Last but not least, there is the question of stability. This is probably the hardest one to answer. We will present results from a paper dealing with this question and although the question is not directly answered there, it hints at the instability of the problem. Thus, we can assume that we are dealing with an ill-posed problem. We will therefore make use of the regularization theory introduced earlier and apply the Tikhonov regularization to our problem. In the last chapter, we will numerically compare this approach to an alternative reconstruction method and see that it indeed leads to a viable means of reconstruction.

Before we move on to the next section, we would like to point out the structural similarity between PAT and another type of tomography, computed tomography (CT). As is explained e.g. in [10], in CT the object is irradiated by x-rays from different angles. The rays leave the source with a specific intensity, pass through the object and are measured on the other side by a detector, typically with a lower final intensity. The information about the intensity loss during the pass-through can be used to reconstruct the object since, as it turns out, this knowledge corresponds to knowing the line integrals of the unknown attenuation function along the ray trajectories. The considered problem in CT is therefore to reconstruct a function $f(x)$, $x \in \mathbb{R}^n$ from its Radon transform defined as

$$(Rf)(y,\theta) := \int_{\mathbb{R}} f(y+t\theta)dt \quad \text{for } \theta \in \mathbb{S}^{n-1} \text{ and } y \in \mathbb{R}^n.$$

Now, our PAT problem can also be reformulated in a similar way. First we define for $n = 2{,}3$ the spherical mean operator

$$(Mf)(y,t) := \frac{1}{|\mathbb{S}^{n-1}|} \int_{\mathbb{S}^{n-1}} f(y+t\theta)d\theta$$

and recall the Poisson-Kirchhoff formula for the solution of our initial value problem in the case $n = 2$,

$$\begin{aligned} p(x,t) &= \frac{1}{2}\frac{\partial}{\partial t}\left[t^2 \frac{1}{|B(x,t)|} \int_{B(x,t)} \frac{f(y)}{\sqrt{t^2-|y-x|^2}} dy \right] \\ &= \frac{1}{2\pi}\frac{\partial}{\partial t}\left[\int_0^t \int_{\partial B(x,s)} \frac{f(y)}{\sqrt{t^2-|y-x|^2}} dS(y)ds \right] \\ &= \frac{1}{2\pi}\frac{\partial}{\partial t}\left[\int_0^t \int_{\mathbb{S}^1} \frac{f(x+sz)\cdot s}{\sqrt{t^2-s^2}} dS(z)ds \right] \\ &= \frac{\partial}{\partial t}\left[\int_0^t \frac{s\cdot(Mf)(x,s)}{\sqrt{t^2-s^2}} ds \right], \end{aligned} \tag{5}$$

or more easily in the case $n = 3$,

$$\begin{aligned} p(x,t) &= \frac{\partial}{\partial t}\left[t\frac{1}{|\partial B(x,t)|}\int_{\partial B(x,t)} f(y)dS(y)\right] \\ &= \frac{\partial}{\partial t}\left[\frac{1}{4\pi t}\int_{\mathbb{S}^2} t^2 \cdot f(x+tz)dS(z)\right] \\ &= \frac{\partial}{\partial t}\left[\, t(Mf)(x,t)\right]. \end{aligned} \tag{6}$$

For $n = 3$ this immediately yields

$$(Mf)(x,t) = \frac{1}{t}\int_0^t p(x,s)ds,$$

hence we see that knowing the acoustic pressure $p(x,t)$ initialized by f is equivalent to knowing the spherical mean of f. To see the same for $n = 2$, we just need to solve an Abel type equation. To this end, we start by noting that it follows from Equation 5 via integration

$$q(x,t) := \int_0^t p(x,s)ds = \int_0^t \frac{s(Mf)(x,s)}{(t^2-s^2)^{\frac{1}{2}}}ds.$$

We use the techniques used in [10] to solve a similar equation. We multiply both sides by $\frac{t}{\sqrt{r^2-t^2}}$ and integrate with respect to t from 0 to r which yields

$$\int_0^r \frac{tq(x,t)}{\sqrt{r^2-t^2}}dt = \int_0^r\int_0^t \frac{ts(Mf)(x,s)}{\sqrt{(r^2-t^2)(t^2-s^2)}}dsdt.$$

Recognizing that the domain of integration on the right-hand side forms a triangle, we can swap the integrals and use that a well-known integral appears such that

$$\begin{aligned} \int_0^r\int_0^t \frac{ts(Mf)(x,s)}{\sqrt{(r^2-t^2)(t^2-s^2)}}dsdt &= \Bigg(\int_0^r\int_s^r\left[\frac{t}{\sqrt{(r^2-t^2)(t^2-s^2)}}dt\right] \\ &\qquad \cdot s(Mf)(x,s)ds\Bigg) \\ &= \frac{\pi}{2}\int_0^r s(Mf)(x,s)ds \end{aligned}$$

Differentiating with respect to r and renaming $r \to t$ and $t \to s$ leads to

$$(Mf)(x,t) = \frac{2}{\pi t}\frac{\partial}{\partial t}\left[\int_0^t \frac{sq(x,s)}{\sqrt{t^2-s^2}}ds\right].$$

Finally, we can plug in the definition of q and observe

$$\begin{aligned}(Mf)(x,t) &= \frac{2}{\pi t}\frac{\partial}{\partial t}\left[\int_0^t \frac{s}{\sqrt{t^2-s^2}}\int_0^s p(x,r)drds\right]\\ &= \frac{2}{\pi t}\frac{\partial}{\partial t}\left[\int_0^t p(x,r)\int_r^t \frac{s}{\sqrt{t^2-s^2}}dsdr\right]\\ &= \frac{2}{\pi t}\frac{\partial}{\partial t}\left[\int_0^t p(x,r)\sqrt{t^2-r^2}dr\right].\end{aligned}$$

Now, using Leibniz's formula for differentiating under the integral sign leaves us with the final formula

$$(Mf)(x,t) = \frac{2}{\pi}\int_0^t \frac{p(x,s)}{(t^2-s^2)^{\frac{1}{2}}}ds.$$

Thus, one can indeed see that the problems of CT and PAT are similar with the difference being that in CT one considers integrals along lines while in PAT integrals over spheres need to be considered. This alternative formulation is indeed useful as it can be used to derive analytical solution formulas for some special observation surfaces, for instance a sphere.

2.3 Uniqueness of Reconstruction

In this section, we present a result dealing with the uniqueness of reconstruction of the initial pressure as in Problem 4. This result first appeared in [7] and we closely follow the approach described there. The only exception will be that we explicitly allow for a finite total measurement time and emphasize where the key assumption made about it is used.

In many applications, the uniqueness of reconstruction is a crucial property (e.g. in the aforementioned medical imaging). Heuristically speaking, there are two major features of our problem which might have an influence on the uniqueness of solution - the total measurement time, and the size and the geometry of the observation surface. The total measurement time is important because as the standard PDE theory tells us, the initial value function f for the wave equation propagates in the solution p with finite speed, namely the speed of sound c (which we assumed to be equal to one). This means that measuring the waves for too short a time period results in a part of f not being visible because the corresponding waves propagating from that part of f simply did not arrive at the observation surface during the measurement. For the case $c = 1$, this suggests taking $T \geqslant \operatorname{diam}(\Omega)$ with $\operatorname{diam}(\Omega) := \sup_{x,y\in\Omega} \|x - y\|$. We will see in the main result of this section, Theorem 6, that such a total measurement time indeed ensures uniqueness. In this theorem, the requirements regarding the observation surface are surprisingly trivial. However, this highlights a difference between theory and practice. Numerical algorithms may nonetheless give better or worse results for different observation surfaces, regardless of the fact that they are all admissible by the uniqueness theorem.

Before we introduce and prove the main theorem, we state a couple of lemmas needed for the proof. Throughout this section, $\Omega \subseteq \mathbb{R}^n$ is a bounded, open, connected set with smooth boundary and such that its closure $\overline{\Omega}$ is strictly convex. For its complement we use the notation $\Omega^\setminus := \mathbb{R}^n \setminus \Omega$. Furthermore, we suppose that the initial pressure function f satisfies $f \in H_0^1(\Omega)$, meaning $f \in H^1(\mathbb{R}^n)$ with $\operatorname{supp}(f) \subseteq \Omega$ compact.

Lemma 1 ([7])**.** Let v be the solution of $v_{tt} - \Delta v = 0$ in $\mathbb{R}^n \times \mathbb{R}$ and let $\chi \in \mathbb{R}^n$, $\delta > 0$ and $\varepsilon > 0$ be such that v is zero on $B_\varepsilon(\chi) \times (-\delta, \delta)$. Then it holds that v is zero on the set

$$\{(x,t) : |x - \chi| + |t| < \delta\}.$$

For the second lemma and also for the proof of the main claim, we define a new metric. For two points $x,y \in \Omega^\setminus$ we define $d(x,y)$ to be the infimum of lengths of all piecewise-C^1-curves in $\Omega^\setminus$ connecting x and y. We note that, since Ω is open, we have $\partial\Omega \subseteq \Omega^\setminus$. Just as $B_\varepsilon(x) = \{y \in \mathbb{R}^n : \|x - y\| < \varepsilon\}$ is the ball in the metric $\|x - y\|$, we set $B_\varepsilon^d(x) := \{y \in \Omega^\setminus : d(x,y) < \varepsilon\}$ to be the ball in the metric $d(x,y)$.

Lemma 2 ([7])**.** Let $\Omega, \Omega^\setminus$ be as above and let v be a smooth solution of

$$\begin{cases} v_{tt} - \Delta v = 0 \text{ in } (\Omega^\setminus \setminus \partial\Omega) \times \mathbb{R} \\ v = \hat{v} \text{ on } \partial\Omega \times \mathbb{R} \end{cases} .$$

If $\chi \in \Omega^\setminus$ and real numbers $t_0 < t_1$ are such that $v(\hat{\chi},t_0) = v_t(\hat{\chi},t_0) = 0$ for any $\hat{\chi} \in B_{t_1-t_0}^d(\chi)$ and also such that $\hat{v} = 0$ on the set $\{(\sigma,t) : \sigma \in \partial\Omega, t_0 \leqslant t \leqslant t_1, d(\sigma,\chi) \leqslant t_1 - t\}$, then it holds that $v(\chi,t) = v_t(\chi,t) = 0$ are equal to zero for any $t_0 \leqslant t \leqslant t_1$.

Although we do not prove this result here, we would like to at least provide a heuristic behind it. Namely, the lemma uses the fact that in case of an obstacle (here in the form of the set Ω), the waves cannot propagate faster than the speed of sound along C^1-trajectories. Therefore, if $v = 0$ at time t_0 for all points reachable from χ in time $t_1 - t_0$ and if the boundary values satisfy $\hat{v} = 0$ at all points and all times such that a value $v \neq 0$ could in theory reach the point χ before the time t_1, then we must have $v = 0$ in χ for all times between t_0 and t_1. Finally, the last ingredient is a geometric result.

Lemma 3 ([7])**.** Let Ω be as before, $\xi \in \partial\Omega$ and $\alpha < \beta$ two positive real numbers. If $K = \overline{\Omega} \setminus B_\beta(\xi)$ is not empty, then the shortest distance (in the usual Euclidean metric) between K and the closure of $B^d_\alpha(\xi)$ is the length (again in the Euclidean metric) of a line segment connecting a point on $\partial\Omega \cap \partial B_\beta(\xi)$ to a point on the boundary of $B^d_\alpha(\xi)$ which lies on $\partial\Omega$.

The main result of this section reads:

Theorem 6 (Uniqueness of reconstruction, [7])**.** Let $\Omega \subseteq \mathbb{R}^n$ be as above and $\Gamma \subseteq \partial\Omega$ be relatively open. Furthermore, let f be as above and p be the solution of the problem

$$\begin{cases} p_{tt} - \Delta p = 0 \text{ in } \mathbb{R}^n \times \mathbb{R} \\ p(x,0) = f(x) \text{ in } \mathbb{R}^n \\ p_t(x,0) = 0 \text{ in } \mathbb{R}^n \end{cases} .$$

Then for any $T \geqslant \operatorname{diam}(\Omega)$ we have that $p(\sigma,t) = 0$ for all $\sigma \in \Gamma$ and all $t \in [0,T]$ implies $f = 0$ in $\mathbb{R}^n$.

Proof. Since f is compactly supported in the open set Ω and Γ is relatively open, we can choose a point $\xi \in \Gamma \subseteq \partial\Omega$ and an $\varepsilon > 0$ such that $f = 0$ in $B_\varepsilon(\xi)$ and $B^d_\varepsilon(\xi) \cap (\partial\Omega \setminus \Gamma) = \emptyset$. This allows us to assume without loss of generality that $\Gamma = B^d_\varepsilon(\xi) \cap \partial\Omega$. The strategy of the proof is to show that if $f = 0$ in $B_r(\xi)$ for an $r \geqslant \varepsilon$, then there is $\delta > 0$ which is independent of r such that actually $f = 0$ in $B_{r+\delta}(\xi)$. This will then immediately imply the statement of the theorem because it means we can just inflate the ball where $f = 0$ so that it eventually covers the whole $\operatorname{supp}(f)$. Suppose $f = 0$ in $B_r(\xi)$ for an $r \geqslant \varepsilon$. Then f is supported in $K \subseteq \overline{\Omega} \setminus B_r(\xi)$. Denoting the Euclidean distance between $B^d_\varepsilon(\xi)$ and K with $\gamma > 0$ and using that we set the speed of sound equal to one, we clearly have $p(x,t) = p_t(x,t) = 0$ for all $(x,t) \in B^d_\varepsilon(\xi) \times (0,\gamma)$. We denote by H^+ the half-space determined by the tangent plane to $\partial\Omega$ at

ξ and directed outwards. Choose $0 < \alpha < \varepsilon$ and $\chi \in B_\alpha(\xi) \cap H^+$. Then p solves the problem

$$\begin{cases} p_{tt} - \Delta p = 0 \text{ in } (\mathbb{R}^n \setminus \Omega) \times [\gamma - \alpha, \infty) \\ p = p_1 \text{ in } (\mathbb{R}^n \setminus \Omega) \times \{\gamma - \alpha\} \\ p_t = p_2 \text{ in } (\mathbb{R}^n \setminus \Omega) \times \{\gamma - \alpha\} \\ p = \hat{p} \text{ on } \partial\Omega \times [\gamma - \alpha, \infty) \end{cases}$$

for functions p_1, p_2 and $\hat{p}$ defined precisely to satisfy this. Now we apply Lemma 2 with $t_0 := \gamma - \alpha$ and $t_1 := \gamma - \alpha + \varepsilon - \alpha$. We observe first $p_1 = p_2 = 0$ in $B^d_\varepsilon(\xi)$ and $\hat{p} = 0$ on $\Gamma \times [\gamma - \alpha, T]$. This implies on one hand $p = 0$ on $B^d_{t_1 - t_0}(\chi)$ since $d(\chi, x) < t_1 - t_0 = \varepsilon - \alpha \implies d(\xi, x) \leqslant d(\xi, \chi) + d(\chi, x) < \alpha + (\varepsilon - \alpha) = \varepsilon$. On the other hand, we also have $p = 0$ on $\{(\sigma, t) : \sigma \in \partial\Omega,\ t_0 \leqslant t \leqslant t_1,\ d(\sigma, \chi) \leqslant t_1 - t\}$ since $d(\chi, \sigma) \geqslant d(\xi, \sigma) - d(\xi, \chi) \geqslant \varepsilon - \alpha$ for all $\sigma \in \partial\Omega \setminus \Gamma$ and $p = 0$ on Γ. Therefore we obtain $p(\chi, t) = 0$ for all $t \in [\gamma - \alpha, \gamma - \alpha + \varepsilon - \alpha)$. We also already showed $p(\chi, t) = 0$ for $0 \leqslant t < \gamma$ so combining these two, the fact that p is even in t and that $\chi \in B_\alpha(\xi) \cap H^+$ was arbitrary gives in total

$$p(\chi, t) = 0 \text{ in } \big(B_\alpha(\xi) \cap H^+\big) \times \big(-(\varepsilon + \gamma - 2\alpha), (\varepsilon + \gamma - 2\alpha)\big).$$

From Lemma 1 it follows that

$$p(x, 0) = f(x) = 0 \text{ for } x \in B_{\varepsilon + \gamma - 2\alpha}(\chi).$$

By triangle inequality, this means $f(x) = 0$ for $x \in B_{\varepsilon + \gamma - 3\alpha}(\xi)$ and so, because $\alpha > 0$ was arbitrary, actually

$$f(x) = 0 \text{ for } x \in B_{\varepsilon + \gamma}(\xi).$$

Now we are just one application of Lemma 3 away from proving our original claim and finishing the proof. Indeed, we start by setting $s := \sup_{\sigma \in \Gamma} \|\xi - \sigma\|$. The strict convexity of $\overline{\Omega}$ implies $s < \varepsilon$. By Lemma 3 it holds that γ is the length of the line segment AB for an $A \in \partial B_r(\xi) \cap \partial\Omega$ and a $B \in \Gamma$. By triangle inequality,

$$\begin{aligned} \varepsilon + \gamma &= \varepsilon + |AB| \\ &= |AB| + |B\xi| + (\varepsilon - |B\xi|) \\ &\geqslant |A\xi| + (\varepsilon - |B\xi|) \\ &\geqslant r + (\varepsilon - s). \end{aligned}$$

We can therefore set $\delta := \varepsilon - s > 0$ and observe that δ is independent of r and satisfies $f = 0$ in $B_{r+\delta}(\xi)$. As already mentioned, one can now take $r_2 := r + \delta$ to be "the new r" and iterate the argument (with the same δ), thereby finishing the proof. We only note that this by construction pushes the set K containing $\operatorname{supp}(f)$ further and further away from Γ (e.g. in the second iteration we would have $K \subseteq \overline{\Omega} \setminus B_{r_2}(\xi)$ with $r_2 > r$). This means that for the same δ to be valid for all r_n we need to know $\hat{p}$ on Γ for a longer and longer time γ. Here the crucial assumption $T \geqslant \operatorname{diam}(\Omega)$ comes in and ensures the validity of the proof. ■

To conclude this section, we just note that the condition $T \geqslant \operatorname{diam}(\Omega)$ is by the above theorem sufficient but may not be always necessary. Indeed, for the case $\Gamma = \partial\Omega$, it was argued in [11] that one just needs to measure long enough so that for every point $x \in \operatorname{supp}(f)$ the signal coming from x reaches some point on the boundary. In other words, in this case the condition $T > \frac{\operatorname{diam}(\Omega)}{2}$ is sufficient for a unique reconstruction.

2.4 Stability of Reconstruction

After the discussion of uniqueness, we devote the following section to the discussion of stability. First, we present a result from [4] and then point out the similarities and the differences between this result and Problem 4 considered in this thesis.

As already mentioned, the problem of reconstructing the initial pressure from the acoustic measurements is unstable. In what follows, we present a result which characterizes the asymptotic behavior of the singular values of a closely-related operator.

To this end, we will work with a distributional formulation

$$\begin{cases} u_{tt} - \Delta u = \delta'(t) f(x) \text{ for } x \in \mathbb{R}^3 \text{ and } t > 0 \\ u(x,t) = 0 \text{ for } x \in \mathbb{R}^3 \text{ and } t < 0 \end{cases} \tag{7}$$

of the underlying initial value problem, where δ denotes the delta distribution and the initial pressure $f \in L^2(\Omega)$ appears in the role of a source term in the wave equation. One can obtain this formulation from the classical one introduced earlier as follows. Given the solution $p : \mathbb{R}^3 \times [0,\infty) \to \mathbb{R}$ of Problem 4, we define a straightforward extension $u : \mathbb{R}^3 \times \mathbb{R} \to \mathbb{R}$ as $u(x,t) := H(t)p(x,t)$ where $H : \mathbb{R} \to \mathbb{R}$ is the Heaviside function satisfying

$$H(t) := \begin{cases} 1, & t \geqslant 0 \\ 0, & t < 0 \end{cases} .$$

Then we get for the second time derivative of u in the distributional sense

$$\partial_{tt}\big(H(t)p(x,t)\big) = \delta'(t)p(x,0^+) + \delta(t)p_t(x,0^+) + H(t)\Delta p(x,t)$$

which implies

$$u_{tt} - \Delta u = H(t)\big(p_{tt} - \Delta p\big) + \delta'(t)f(x).$$

Using the definition of the Heaviside function and the fact that p satisfies Problem 4, one arrives at the formulation in Equation 7. As is proven in [4], the advantage of this formulation is that it allows for a closed expression of the solution in the temporal frequency domain. It holds

$$\check{u}(x,\omega) = -\int_{\mathbb{R}^3} \frac{i\omega}{4\pi\sqrt{2\pi}} \frac{e^{i\omega|x-y|}}{|x-y|} f(y)dy \tag{8}$$

with $\check{u}$ being the inverse Fourier transform of u with respect to the time variable. This observation leads to the definition of the time-integrated photoacoustic operator $\check{\mathbf{T}} : L^2(\Omega_\varepsilon) \to L^2(\partial\Omega \times \mathbb{R})$

$$[\check{\mathbf{T}}f](x,\omega) := \frac{1}{4\pi\sqrt{2\pi}} \int_{\mathbb{R}^3} \frac{e^{i\omega|x-y|}}{|x-y|} f(y)dy$$

with $\Omega_\varepsilon := \{x \in \Omega : \mathrm{dist}(x,\partial\Omega) > \varepsilon\}$ and some $\varepsilon > 0$. It is called time-integrated because, compared to Equation 8, there is a factor $-i\omega$ missing, which corresponds to integration in the time domain. The key results are the following two theorems for which we will not provide proofs since these would be out of the scope of this thesis.

Theorem 7 ([4])**.** Let $\Omega \subseteq \mathbb{R}^3$ be a convex, bounded domain with smooth boundary. Then the time-integrated operator $\check{\mathbf{T}}$ is bounded with a well-defined adjoint $\check{\mathbf{T}}^*$ and $\check{\mathbf{T}}^*\check{\mathbf{T}} : L^2(\Omega_\varepsilon) \to L^2(\Omega_\varepsilon)$ is given by

$$[\check{\mathbf{T}}^*\check{\mathbf{T}}f](x) = \int_\Omega K(x,y)f(y)dy$$

with $K \in L^2(\Omega_\varepsilon \times \Omega_\varepsilon)$. In particular, we have that $\check{\mathbf{T}}^*\check{\mathbf{T}}$ is a Hilbert-Schmidt operator and therefore compact.

Additionally, $\check{\mathbf{T}}^*\check{\mathbf{T}}$ is clearly self-adjoint. Therefore, the spectral theorem for compact, self-adjoint operators yields a decreasing sequence of eigenvalues $\lambda_n \to 0$. Now, $\check{\mathbf{T}}^*\check{\mathbf{T}}$ being compact implies that $\check{\mathbf{T}}$ is compact too and therefore admits a singular value decomposition. Since the singular values σ_n of $\check{\mathbf{T}}$ are related to the eigenvalues λ_n of $\check{\mathbf{T}}^*\check{\mathbf{T}}$ via $\sigma_n = \sqrt{\lambda_n}$, one just needs to analyze the asymptotic behavior of λ_n. This is the subject of the following theorem.

Theorem 8 ([4]). Let $\Omega \subseteq \mathbb{R}^3$ be a convex, bounded domain with smooth boundary. Then there are constants $C_1, C_2 > 0$ such that the eigenvalues λ_n of $\check{\mathbf{T}}^*\check{\mathbf{T}} : L^2(\Omega_\varepsilon) \to L^2(\Omega_\varepsilon)$ satisfy

$$C_1 n^{-\frac{2}{3}} \leqslant \lambda_n \leqslant C_2 n^{-\frac{2}{3}}$$

for all $n \in \mathbb{N}$.

Clearly, we get $\sqrt{C_1} n^{-\frac{1}{3}} \leqslant \sigma_n \leqslant \sqrt{C_2} n^{-\frac{1}{3}}$ and so we obtain a characterization for the asymptotic behavior of the singular values of the time-integrated photoacoustic operator. However, compared to the classical photoacoustic operator $\mathbf{P}$ which maps the initial pressure directly to the solution of the wave equation on $\partial\Omega$ and which will be studied in more detail in the next section, the operator $\check{\mathbf{T}}$ consists of two additional operations - the inverse Fourier transform and integration, both with respect to time. Looking at the situation from the opposite angle, one obtains the operator $\mathbf{P}$ from $\check{\mathbf{T}}$ by applying an additional Fourier transform and differentiating. The Fourier transform $\mathscr{F} : L^2(\Omega) \to L^2(\Omega)$ is a well-behaved unitary operator but differentiating is less well-behaved. Therefore, the characterization given in Theorem 8 cannot be simply used to characterize the ill-posedness of the classical photoacoustic operator. However, at the moment, there seems to be no result which would extend the characterization of $\check{\mathbf{T}}$ to $\mathbf{P}$.

2.5 Tikhonov Regularization of the Photoacoustic Problem

In this section, we first re-define Problem 4 using a bounded, linear operator and then show how this allows us to apply the Tikhonov regularization discussed in Section 1.4.

The theoretical problem is to reconstruct the initial pressure function f in Ω from the perfect measurements $g \in L^2(\Gamma \times [0,T])$ satisfying $g(\sigma,t) = p(\sigma,t)$ in $\Gamma \times [0,T]$. Theorem 6 tells us that, under quite mild conditions, this is possible in a unique way. However, this might be an idealized situation since in practice we do not have perfectly accurate data at our disposal. Instead, due to measurement errors, we deal with $g^\delta \in L^2(\Gamma \times [0,T])$ - a noisy version of our data satisfying

$$\|g - g^\delta\|_{L^2(\Gamma\times[0,T])} \leqslant \delta.$$

Since we do not have stability of reconstruction, applying a reconstruction procedure to the noisy data as if it was the exact data might not lead to a good result. Moreover, it may also be the case that due to some reasons we cannot conduct the measurements for a sufficiently long time or that the observation surface is too far/does not surround the object very well. All these factors make the problem even more ill-posed and the reconstruction more difficult and unstable. We would therefore like to apply the theory of Tikhonov regularization developed in the first part. For this, we first need to formulate the problem as an equation involving a bounded operator between Hilbert spaces. This motivates the following definition.

Definition 4. Let $\Omega \subseteq \mathbb{R}^n$ be as before, $\Gamma \subseteq \partial\Omega$ relatively open and $T \geqslant \operatorname{diam}(\Omega)$. For $f \in H_0^1(\Omega)$ we denote by p the solution of Problem 4 with $c \equiv 1$

$$\begin{cases} p_{tt} - \Delta p = 0 \text{ in } \mathbb{R}^n \times (0,\infty) \\ p(x,0) = f(x) \text{ in } \Omega \\ p(x,0) = 0 \text{ in } \mathbb{R}^n \setminus \Omega \\ p_t(x,0) = 0 \text{ in } \mathbb{R}^n \end{cases}.$$

Then the operator

$$\mathbf{P} : H_0^1(\Omega) \to L^2(\Gamma \times [0,T])$$

mapping f to $\mathbf{P}(f) := p|_{\Gamma \times [0,T]}$ is called **the photoacoustic operator**.

First of all, we note that with the specific choice of Γ and T the photoacoustic operator is injective by Theorem 6. Second of all, the two spaces $H_0^1(\Omega)$ and $L^2(\Gamma \times [0,T])$ are Hilbert spaces when considered together with their respective inner products

$$\langle f_1, f_2 \rangle_{H_0^1(\Omega)} := \int_\Omega (\nabla f_1) \cdot (\nabla f_2)\, dx$$

and

$$\langle g_1, g_2 \rangle_{L^2(\Gamma \times [0,T])} := \int_0^T \int_\Gamma g_1 \cdot g_2 \, dS\, dt.$$

We will also work with the norm $\|\cdot\|_{H^1(\Omega)}$ coming from the inner product

$$\langle f_1, f_2 \rangle_{H^1(\Omega)} := \int_\Omega f_1 \cdot f_2 \, dx + \int_\Omega (\nabla f_1) \cdot (\nabla f_2)\, dx.$$

Finally, the next theorem from [1] shows that $\mathbf{P}$ is bounded and thus the theory of Tikhonov regularization applies.

Theorem 9 ([1])**.** For $\Omega \subseteq \mathbb{R}^n$, $\Gamma \subseteq \partial\Omega$ and $T > 0$ as before, the photoacoustic operator $\mathbf{P}$ is bounded.

Proof. We start by taking an arbitrary $f \in H_0^1(\Omega)$ and again using p to denote the solution of the wave equation with f as the initial value. This allows us to write

$$\begin{aligned}
\|\mathbf{P}(f)\|^2_{L^2(\Gamma\times[0,T])} \leqslant \|\mathbf{P}(f)\|^2_{L^2(\partial\Omega\times[0,T])} \\
&= \int_0^T \int_{\partial\Omega} P(f)(\sigma,t)^2 \, dS(\sigma) \, dt \\
&= \int_0^T \|p(\cdot,t)\|^2_{L^2(\partial\Omega)} \, dt.
\end{aligned} \tag{9}$$

Since the trace operator $H^1(\Omega) \to L^2(\partial\Omega)$ is bounded with norm equal to a constant $C_{\text{trace}} > 0$, we would like to show $p(\cdot,t) \in H^1(\Omega)$, or actually $p(\cdot,t) \in H^1(\mathbb{R}^n)$, for every fixed t and then bound $\|p(\cdot,t)\|_{H^1(\mathbb{R}^n)}$ by the norm of f. To this end, we first define the quantity

$$E(t) := \int_{\mathbb{R}^n} (p_t)^2 + |\nabla p|^2 \, dx$$

and observe that $E(t)$ is constant in time. In fact, integrating the second term by parts yields

$$\int_{\mathbb{R}^n} |\nabla p|^2 \, dx = -\int_{\mathbb{R}^n} p \cdot \Delta p \, dx.$$

Therefore we get for the time derivative of E

$$E'(t) = \int_{\mathbb{R}^n} 2p_{tt}p_t - p_t\Delta p - p\Delta p_t \, dx.$$

Leveraging integration by parts for a second time shows that the last two terms are equal and therefore

$$E'(t) = 2\int_{\mathbb{R}^n} p_t(p_{tt} - \Delta p) \, dx = 0$$

since p satisfies the wave equation. Thus $E(t) = E(0) = \|f\|^2_{H_0^1(\Omega)}$ and so for any $t \in [0,T]$ we obtain the two inequalities

$$\int_{\mathbb{R}^n} p_t(x,t)^2 \, dx \leqslant \|f\|^2_{H_0^1(\Omega)} \tag{10}$$

and

$$\|p(\cdot,t)\|_{H_0^1(\mathbb{R}^n)} \leqslant \|f\|_{H_0^1(\Omega)}. \tag{11}$$

It holds $\|\cdot\|^2_{H^1(\mathbb{R}^n)} = \|\cdot\|^2_{H^1_0(\mathbb{R}^n)} + \|\cdot\|^2_{L^2(\mathbb{R}^n)}$ and so the remaining part is to bound $\|p(\cdot,t)\|_{L^2(\mathbb{R}^n)}$ by $\|f\|_{H^1_0(\Omega)}$. To achieve this, we employ the fundamental theorem of calculus, the Cauchy-Schwarz inequality and Inequality 10 in this order and estimate

$$\begin{aligned}
\int_{\mathbb{R}^n} \big(p(x,t) - p(x,0)\big)^2 \, dx &= \int_{\mathbb{R}^n} \left(\int_0^t p_t(x,s) \, ds \right)^2 dx \\
&\leqslant t \int_0^t \int_{\mathbb{R}^n} p_t(x,s)^2 \, dxds \\
&\leqslant t^2 \|f\|^2_{H^1_0(\Omega)} \\
&\leqslant T^2 \|f\|^2_{H^1_0(\Omega)}.
\end{aligned}$$

We can now use that f is compactly supported so $f \in H^1(\Omega)$ and that the norms $\|\cdot\|_{H^1(\Omega)}$ and $\|\cdot\|_{H^1_0(\Omega)}$ are equivalent to get

$$\begin{aligned}
\|p(\cdot,t)\|^2_{L^2(\mathbb{R}^n)} &= \int_{\mathbb{R}^n} p(x,t)^2 \, dx \\
&\leqslant 2 \int_{\mathbb{R}^n} \big(p(x,t) - p(x,0)\big)^2 \, dx + 2 \int_{\mathbb{R}^n} p(x,0)^2 \, dx \\
&\leqslant 2T^2 \|f\|^2_{H^1_0(\Omega)} + 2\|f\|^2_{L^2(\Omega)} \\
&\leqslant C(T) \|f\|^2_{H^1_0(\Omega)}
\end{aligned}$$

for a constant $C(T)$ depending on T. Combining this and Inequality 11 results in

$$\|p(\cdot,t)\|^2_{H^1(\mathbb{R}^n)} \leqslant \big(C(T)+1\big) \|f\|^2_{H^1_0(\Omega)}. \tag{12}$$

This enables us to finish what we started in Inequality 9, namely

$$\begin{aligned}
\|\mathbf{P}(f)\|^2_{L^2(\Gamma\times[0,T])} &\leqslant \int_0^T \|p(\cdot,t)\|^2_{L^2(\partial\Omega)} \, dt \\
&\leqslant C^2_{\text{trace}} \int_0^T \|p(\cdot,t)\|^2_{H^1(\mathbb{R}^n)} \, dt \\
&\leqslant T C^2_{\text{trace}} \big(C(T)+1\big) \|f\|^2_{H^1_0(\Omega)},
\end{aligned}$$

thereby finishing the proof. ■

We now come back to the situation from the beginning of this section in which we only have the noisy data g^δ instead of the perfect data g. First of all, it is not guaranteed that $g^\delta \in ran(\mathbf{P})$ and so the equation

$$\mathbf{P}f = g^\delta$$

might not have a solution. One might therefore try to compute $\mathbf{P}^\dagger g^\delta$ by solving the normal equation

$$\mathbf{P}^*\mathbf{P}f = \mathbf{P}^* g^\delta.$$

However, this might still not lead to a viable reconstruction because of the noisiness of the data. A better way might be to consider the Tikhonov-regularized version of the equation and solve

$$(\mathbf{P}^*\mathbf{P} + \alpha I)f = \mathbf{P}^* g^\delta$$

with I being the identity on $H_0^1(\Omega)$ and $\alpha > 0$. Theorem 4 tells us that this is equivalent to minimizing the functional

$$\begin{aligned} f &\mapsto \|\mathbf{P}f - g^\delta\|^2_{L^2(\Gamma\times[0,T])} + \alpha\|f\|^2_{H_0^1(\Omega)} \\ &= \int_0^T \int_\Gamma (\mathbf{P}f - g^\delta)^2 \, dSdt \; + \alpha \int_\Omega |\nabla f|^2 \, dx. \end{aligned} \tag{13}$$

The last expression sheds some light onto what is happening when we compute the Tikhonov-regularized solution. Let us denote the regularized solution found this way with f_α^δ. The first so-called data fidelity term makes sure that $\mathbf{P}f_\alpha^\delta$ is reasonably close to g^δ (in the L^2-sense). One could say that it makes f_α^δ “a plausible guess” for the reconstruction. The second so-called penalty term imposes a condition on the regularity of the solution with α quantifying the extent to which the regularity is taken into account. Since what is minimized is the sum of the two, the result is a compromise between the fit and the smoothness of the solution. We emphasize again that the contribution of the two terms is determined by the parameter $\alpha \in [0,\infty)$. For $\alpha = 0$ it is the non-regularized solution which only takes into account the fit. Meanwhile, for $\alpha \to \infty$ we would have $\|f_\alpha^\delta\|_{H_0^1(\Omega)} \to 0$ since the data fidelity term would become less and less relevant.

Before moving on to the next section, we would like to briefly address the issue of evaluating the adjoint of $\mathbf{P}$. In [1], $\mathbf{P}^*h$ is computed explicitly for $h \in C^\infty(\Gamma \times [0,T])$ and essentially turns out to be a solution of a boundary value problem for the wave equation with h playing the role of the boundary values. Nonetheless, it is important to mention that in practice it is not always necessary to compute the adjoint in this way. In fact, since solving the problem numerically anyway requires discretizing the functions and spaces involved, what one obtains is usually a discretized version of the operator in the form of a finite-dimensional matrix. Taking the adjoint of a matrix is far easier and in our case also sufficient as a substitute for the adjoint of the original continuous operator. We will see this in more detail in the next chapter.

2.6 Time Reversal as a Method of Reconstruction

After establishing how to apply Tikhonov regularization to the photoacoustic problem in the previous section, we describe in this section the method of reconstruction via time reversal which will serve us as a benchmark for evaluating the solution method based on Tikhonov regularization.

One of the most frequently used methods of reconstruction in PAT is the time reversal method. If we assume that $\Gamma = \partial\Omega$ is a closed surface, then it constitutes a reliable means of reconstruction for practically any geometry of the domain Ω. In what follows, we would like to introduce this method and we start by highlighting two properties of the wave equation. Namely, consider an arbitrary function w satisfying

$$w_{tt} - \Delta w = 0 \text{ in } \mathbb{R}^n \times \mathbb{R}$$

and define $\tilde{w}$ via $\tilde{w}(x,t) := w(x,-t)$. Then $\tilde{w}$ also satisfies the wave equation in $\mathbb{R}^n \times \mathbb{R}$ because

$$\tilde{w}_{tt}(x,t) - (\Delta\tilde{w})(x,t) = (-1)^2 w_{tt}(x,-t) - (\Delta w)(x,-t) = 0$$

by the chain rule. The second ingredient is Huygens' principle for the wave equation in odd dimensions. It states that if $w(x,0)$ is compactly supported, then the waves will leave any bounded domain $B \subseteq \mathbb{R}^n$ in finite time, meaning $w(x,t) = 0$ for all $x \in B$ and $t > T = T(B)$ depending on B. For $n = 3$, we can already see this by inspecting the Poisson-Kirchhoff formula in Equation 6. This does not hold in general for even dimensions as we can also confirm by inspecting the Poisson-Kirchhoff formula in Equation 5. Nonetheless, also in even dimensions one may derive at least some decay properties of the solution w in bounded domains.

Using these two properties, one may propose the following method of reconstruction. Consider again Problem 4 but for now let us assume we have the data $g(\sigma,t) = p(\sigma,t)$ for $\sigma \in \Gamma = \partial\Omega$ and $t \in [0,T]$ such that $\partial\Omega$ is a closed surface and $T \geqslant \mathrm{diam}(\Omega)$ satisfies $p(x,t) = 0$ for $x \in \Omega$, $t \geqslant T$. For odd n the last condition means we wait till the waves fully propagate outside of Ω, while for even n we can at least approximately replace this by p being sufficiently small for all later times. We denote by $\tilde{p}$ the unique solution of the problem

$$\begin{cases} \tilde{p}_{tt} - \Delta \tilde{p} = 0 \text{ in } \Omega \times (0,T) \\ \tilde{p}(x,0) = 0 \text{ in } \Omega \\ \tilde{p}_t(x,0) = 0 \text{ in } \Omega \\ \tilde{p}(\sigma,t) = g(\sigma, T-t) \text{ on } \Gamma \times [0,T] \end{cases} \tag{14}$$

Then clearly $\tilde{p}(x,t) = p(x,T-t)$ because the latter solves the problem and the problem has a unique solution. Since $\tilde{p}$ is just the time-reversed p, this means

$$\tilde{p}(x,T) = p(x,0) = f(x).$$

Hence, all we need to do is to solve Problem 14 for $\tilde{p}$ which is possible by standard numerical methods. Often, this method serves as a benchmark for assessing the quality of other reconstruction methods. This will be its use case for us too as we will compare it with the reconstruction using Tikhonov regularization in the next chapter. However, before that, we have to address one difference of the setup described above compared to our situation. Namely, we do not necessarily have $\Gamma = \partial\Omega$. In the case $\Gamma \subsetneq \partial\Omega$, we lack the information about the solution corresponding to the unobserved part of the boundary. For Problem 14 to be numerically solvable for example by the standard finite element method, one has to decide about the behavior on the whole boundary. Depending on the numerical method chosen, there might be different artifacts appearing in the reconstruction.

3. Numerical Implementation

3.1 Numerical Setup

3.1.1 K-Wave and the Domain of Computation

For the implementation of the photoacoustic operator we resort to the well-known k-Wave implementation. Therefore, in this section, we would like to offer a brief description of the computational methods it employs and then also of our computational setup. We refer to [12] for more details.

First of all, instead of the standard wave equation coupled with initial conditions, k-Wave tackles an equivalent first-order system of the type

$$\begin{cases} u_t = -\nabla \text{ in } D \times (0,T) \\ p_t = -\nabla \cdot u \text{ in } D \times (0,T) \\ p(x,0) = f(x) \text{ in } D \\ p_t(x,0) = 0 \text{ in } D \end{cases}$$

where $u : D \to \mathbb{R}^2$ is the acoustic particle velocity and $p : D \to \mathbb{R}$ is the acoustic pressure. From now on, D denotes our computational domain. The mathematical domain Ω considered in the previous sections is a strict subset of the computational domain D since, as we describe below, the computations require modeling the ambient space around Ω, too. One could therefore say that D serves as a substitute for the space $\mathbb{R}^2$ of which Ω was a strict subset in our theoretical considerations. However, there is a significant difference between this setup and the original formulation of our problem. Namely, the computational domain D is necessarily finite. This is in contrast to the physical case where the waves theoretically propagate through the infinite space without any boundaries. This means that one needs to prescribe boundary conditions at ∂D, regardless of the computational method. Using incorrect assumptions may however harm our solution. For example, imposing incorrect Dirichlet conditions may cause waves to reflect back into the domain instead of them simply propagating outside. The remedy k-Wave uses for this is the so-called perfectly matched layer (PML). PML is a thin layer near the actual boundary of D inside which an extra term causing anisotropic attenuation is added to the first-order system. It is also assumed that p can be written as $p = p^{(x_1)} + p^{(x_2)}$ with $p^{(x_j)}$ being a function of x_j solely (we use the notation $x = (x_1,x_2) \in \mathbb{R}^2$) and similarly for u. The actual system of equations k-Wave solves is then

$$\begin{cases} u_t = -\nabla p - au \text{ in } D \times (0,T) \\ p_t^{(x_1)} = -u_{x_1}^{(x_1)} - a_1 p^{(x_1)} \text{ in } D \times (0,T) \\ p_t^{(x_2)} = -u_{x_2}^{(x_2)} - a_2 p^{(x_2)} \text{ in } D \times (0,T) \\ p(x,0) = f(x) \text{ in } D \\ p_t(x,0) = 0 \text{ in } D \end{cases} \tag{15}$$

where $a = (a_1,a_2) : D \to \mathbb{R}^2$ is the anisotropic absorption non-zero only in the PML and we use the notation g_{x_j} for the partial derivative of a function g with respect to x_j, similarly as with the time variable t.

To solve Problem 15, k-Wave employs a pseudospectral method. The spatial gradients are computed in the frequency space by leveraging the fact that p_{x_j} is just the inverse Fourier transform of $ik_j\hat{p}(k,t)$ (here we use $\hat{p}$ to denote the Fourier transform of p along the spatial dimensions and, as before, $k = (k_1,k_2)$) and that the fast Fourier transform (FFT) is numerically cheap to execute. For the time evolution it uses finite differences with leapfrog time stepping enriched by a multiplication term of the form

$$sinc\left(\frac{|k|\Delta t}{2}\right)$$

in the frequency space which improves stability of the computation. The boundary conditions are then set to be periodic (a wave leaving through one part of the boundary enters through the opposite part) but with the anisotropic attenuation in the PML this is an admissible approach.

Finally, we describe the domain of computation. We will work on a square grid of size 256 x 256 which we, as already mentioned, denote by D. The slightly smaller square of size 206 x 206 around the midpoint will play the role of the domain Ω and the 128 x 128 square around the midpoint will be the support of the function f we would like to reconstruct. As a mathematical domain, Ω will represent the unit square $[0,1]^2$. The PML encloses the boundary of D and has thickness of 15 grid points. As the observation surface $\Gamma \subseteq \partial\Omega$ we chose the left and the lower edge of the square Ω. Furthermore, we set $\Delta t = 0.0003$ for the length of a time step and $\Delta x = 0.001$ for the length of a spatial step to ensure stability of the scheme. The whole computational domain is shown in Figure 3.

3.1.2 DS Basis

In this section, we describe our choice of the basis functions used for approximating the true initial pressure.

The numerical method explained above is used to evaluate the photoacoustic operator for a given initial pressure function discretized on our finite grid. Given the acoustic pressure data $g \in L^2(\Gamma \times [0,T])$, Tikhonov regularization suggests we shall look for $f \in H_0^1(\Omega)$ which for $\alpha > 0$ minimizes

$$||\mathbf{P}f - g||^2_{L^2(\Gamma\times[0,T])} + \alpha||f||^2_{H_0^1(\Omega)}.$$

However, a search through the whole space $H_0^1(\Omega)$ is infeasible. Therefore, we intend to discretize also the operator itself, meaning we evaluate it only on a finite number of basis functions $\{\psi_i\}_{i=1}^N$ with $\psi_i \in H_0^1(\Omega)$ for every i. Then, we will look for a linear combination $\sum_{i=1}^N c_i(g)\psi_i$ which minimizes

$$||\mathbf{P}h - g||^2_{L^2(\Gamma\times[0,T])} + \alpha||h||^2_{H_0^1(\Omega)} \text{ for } h \in span\{\psi_i\}_{i=1}^N.$$

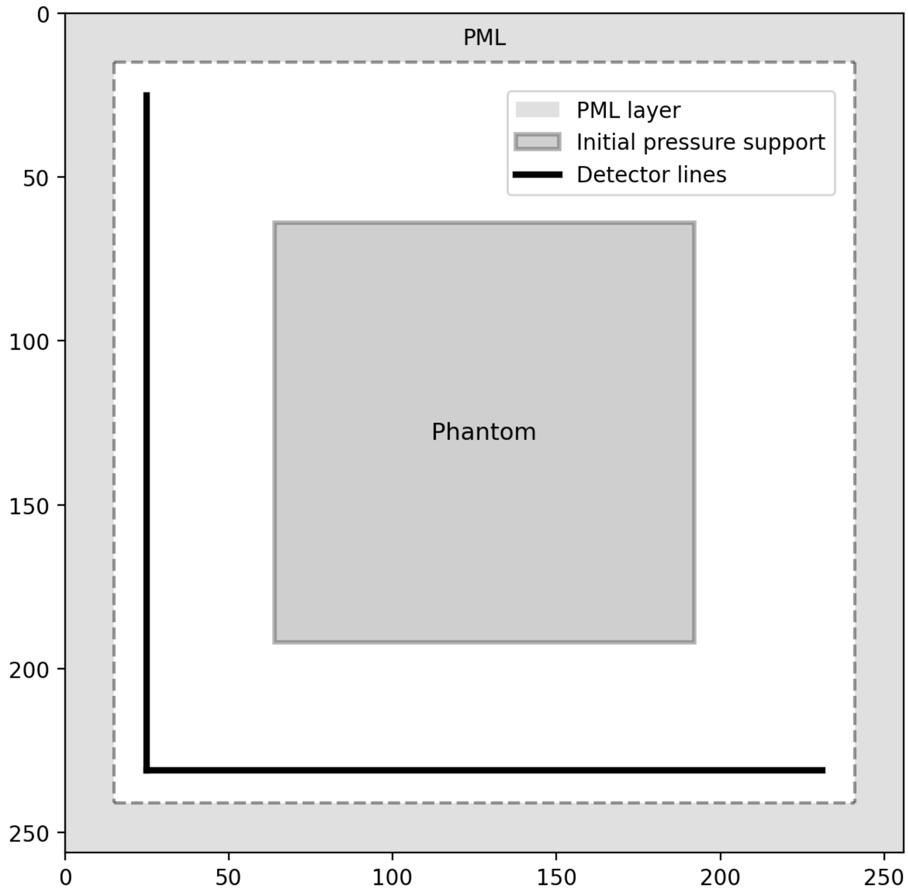

Figure 3
Computational domain

This means that the basis functions should be chosen carefully so that they can express a wide enough class of initial pressure functions. We made the choice to work with the functions

$$\psi_{k,\ell}(x,y) := 2\sin(k\pi x)\sin(\ell\pi y)$$

for $x,y \in [0,1]$ and $k,\ell \geqslant 1$. The discrete samples of these functions constitute the so-called Discrete sine (DS) basis and the representation of a function f as a linear combination of these functions is the Discrete sine transform (DST) of f. A quick calculation verifies that $\psi_{k,\ell}$ solve the eigenvalue equation

$$\begin{cases} -\Delta\psi_{k,\ell} = \lambda_{k,\ell}\psi_{k,\ell} \text{ in } \Omega \\ \psi_{k,\ell} = 0 \text{ on } \partial\Omega \end{cases}$$

with $\lambda_{k,\ell} := \pi^2(k^2+\ell^2)$. Since $-\Delta$ is an elliptic symmetric operator, Theorem 1 in Section 6.5.1 in [6] implies that $\{\psi_{k,\ell}\}_{k,\ell=1}^{\infty}$ form an orthonormal basis of $L^2(\Omega)$. A closely related transform is the so-called Discrete cosine transform

(DCT) which employs functions of the form

$$2\cos(k\pi x)\cos(\ell\pi y).$$

The DCT was first proposed in 1972 and is nowadays still widely used in signal processing and signal compression, for example in formats such as JPEG, MPEG and MP3. It is mathematically equivalent to the Discrete Fourier transform of data with even symmetry. The DST is much less used. Nonetheless, our decision to use the DST was quite natural since these functions are smooth and vanish on the boundary which nicely fits into our H_0^1-framework. We found that the DS functions with $1 \leqslant k,\ell \leqslant 70$ are able to express initial pressure functions f of practical interest with sufficient accuracy. This results in 4900 functions which are sampled on the 128 x 128 grid. For more details on DCT and DST, we refer to [3].

3.1.3 Linear System of Equations

After introducing all the necessary ingredients, we present in this section the exact linear system of equations we solve to obtain an approximation of the initial pressure.

The method of reconstruction is now the following. First, we assemble and store the basis functions. With each basis function acting as initial pressure, we then compute the acoustic data. Storing this in one array gives us a matrix $\overline{P} \in \mathbb{R}^{(\text{#detector pixels} \cdot \text{#time steps}) \times \text{#basis functions}}$ - a discretized version of the photoacoustic operator. Similarly, we obtain a vector $\overline{g} \in \mathbb{R}^{\text{#detector pixels} \cdot \text{#time steps}}$ of the acoustic waves generated by the unknown initial pressure we wish to reconstruct. We obtain a linear system of equations

$$\overline{P}\overline{f} = \overline{g}$$

with $\overline{f} \in \mathbb{R}^{\text{#basis functions}}$. Now, the classical approach outlined in the first chapter suggests choosing a parameter $\alpha > 0$ and working with the regularized normal equation

$$(\overline{P}^*\overline{P} + \alpha\overline{I})\overline{f} = \overline{P}^*\overline{g}$$

where $\overline{I} \in \mathbb{R}^{\text{#basis functions} \times \text{#basis functions}}$ is simply the identity matrix playing the role of the identity operator on (the subset of) $H_0^1(\Omega)$ and $\overline{P}^*$ is the transpose of the matrix $\overline{P}$. However, there is also an alternative way to regularize the system. To this end, we first look again at the continuous version of the regularized normal equation

$$(\mathbf{P}^*\mathbf{P} + \alpha I)f = \mathbf{P}^*g.$$

Since we anyway work only in the subspace $span\{\psi_{k,\ell}\}_{k,\ell=1}^{70} \subseteq H_0^1(\Omega)$, we may require that the reconstructed $f \in span\{\psi_{k,\ell}\}_{k,\ell=1}^{70}$ satisfy

$$\langle \mathbf{P}^*\mathbf{P}f, h\rangle_{H_0^1(\Omega)} + \alpha\langle f, h\rangle_{H_0^1(\Omega)} = \langle \mathbf{P}^*g, h\rangle_{H_0^1(\Omega)} \quad \forall h \in span\{\psi_{k,\ell}\}_{k,\ell=1}^{70}$$

which is equivalent to

$$\langle \mathbf{P}^*\mathbf{P}f, \psi_{k,\ell}\rangle_{H_0^1(\Omega)} + \alpha\langle f, \psi_{k,\ell}\rangle_{H_0^1(\Omega)} = \langle \mathbf{P}^*g, \psi_{k,\ell}\rangle_{H_0^1(\Omega)}$$

for all $1 \leqslant k,\ell \leqslant 70$. Using the defining property of the adjoint, this is in turn equivalent to

$$\langle \mathbf{P}f, \mathbf{P}\psi_{k,\ell}\rangle_{L^2(\Gamma\times[0,T])} + \alpha\langle f, \psi_{k,\ell}\rangle_{H_0^1(\Omega)} = \langle g, \mathbf{P}\psi_{k,\ell}\rangle_{L^2(\Gamma\times[0,T])}$$

for all $1 \leqslant k,\ell \leqslant 70$. Using $f \in span\{\psi_{k,\ell}\}_{k,\ell=1}^{70}$, it is an easy exercise to see that in our discretized setting this results, up to scaling by the spatial and time steps since these are discretized integrals, in the linear system of equations

$$(\overline{P}^*\overline{P} + \alpha\overline{S})\overline{f} = \overline{P}^*\overline{g}$$

where $\overline{P}$ is the same matrix as before and $\overline{S}$ is the so-called stiffness matrix whose components are the inner products $\langle \psi_{k,\ell}, \psi_{k',\ell'}\rangle_{H_0^1(\Omega)}$ for every pair of basis functions. The advantage is that for our choice of basis functions the matrix $\overline{S}$ has a special form. Namely, since the basis functions are eigenfunctions of the Laplacian, we get

$$\begin{aligned}
\langle \psi_{k,\ell}, \psi_{k',\ell'}\rangle_{H_0^1(\Omega)} &= \int_\Omega \nabla\psi_{k,\ell} \cdot \nabla\psi_{k',\ell'}\, dx \\
&= \int_\Omega \psi_{k,\ell} \cdot (-\Delta\psi_{k',\ell'})\, dx \\
&= \delta_{k,k'}\,\delta_{\ell,\ell'}\,\pi^2(k^2+\ell^2)
\end{aligned}$$

where $\delta_{\cdot,\cdot}$ is the Kronecker delta. Therefore, we see that the penalty matrix is again diagonal. However, in this case the basis functions corresponding to higher frequencies are penalized more relative to the penalty imposed on the lower frequencies.

We decided to proceed with the latter approach and will present the results below. Nonetheless, both approaches yield good reconstruction results.

3.2 Reconstruction with Sufficient Measurement Time

Below we present the reconstruction results. We start with the case of total measurement time satisfying the assumption of Theorem 6 and thus sufficient for unique reconstruction. We let k-Wave automatically choose a sufficient measurement time to be $T = 1207 \cdot dt$. Both in this and in the subsequent section we will work with two different phantoms. The first one is the classical Shepp-Logan phantom typically used for reconstruction experiments. The other phantom consists of disks placed on the diagonal connecting the bottom left corner of the domain with the upper right one as well as a couple of other off-diagonal disks. We designed this phantom specifically to study the effects of shorter measurement time in the next section. For both phantoms, we work with the regularization parameter $\alpha = 10^{-14}$. We say more about the choice of this α at the end of this section. As already indicated, we intend to use the reconstruction based on time reversal as a benchmark to assess our method. It is important to note that for a general function $f \in H_0^1(\Omega)$, we can project it onto $span\{\psi_{k,\ell}\}_{k,\ell=1}^{70}$ only up to a certain error. Hence the reconstruction from the acoustic pressure data can only come as close to the original function as its projection does, at least in the L^2-sense. Therefore, we will show for every result four pictures:

- the true initial pressure in the upper left corner
- the projection onto $span\{\psi_{k,\ell}\}_{k,\ell=1}^{70}$ in the upper right corner
- our reconstruction based on Tikhonov regularization in the bottom left corner
- the reconstruction based on time reversal in the bottom right corner.

The results for the reconstruction of the Shepp-Logan phantom can be seen in Figure 4. Interestingly, at least when it comes to the minimum and maximum values, the Tikhonov reconstruction seems more accurate than the initial DST-projection. This is because the projection minimizes the L^2-error and not the point-wise error. In Table 1 presented at the end of this section, we will see that the DST-projection indeed wins in the L^2-sense. The Tikhonov reconstruction smooths out the sharpest edges of the phantom but otherwise yields a very good result. The smoothing effect stems directly from our penalty term. As shown in Equation 13, the regularization penalizes large gradients. Since we did not smooth out the phantom beforehand, the edges of the ellipses have very large gradients and so are one of the features penalized the most which translates into the smoothing. We will be able to observe the same effect also in the other phantom. A good reconstruction is achieved by the time reversal method as well where the contrast might be a bit better in the smallest features but where also slight artifacts inside as well as outside of the phantom are present. Additionally, the scaling is much more off. Finally, one notices

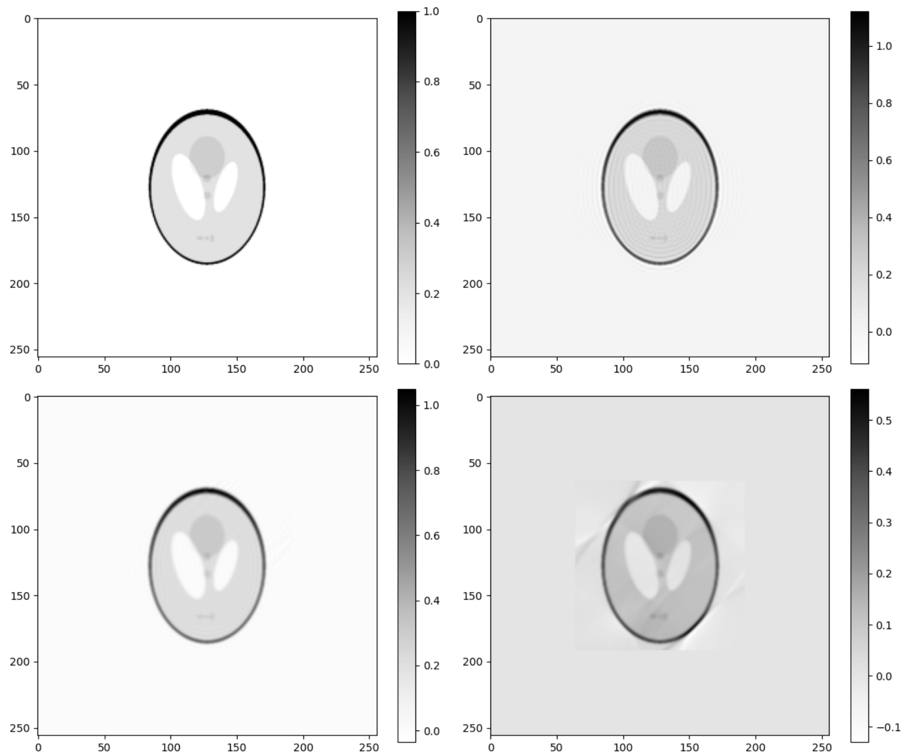

Figure 4
Reconstruction results for the Shepp-Logan phantom

that for the time reversal reconstruction only the inner 128x128 square was used and subsequently zero-padded. We did this to make it “fair” - since we know what the support of the image is, we can use this a priori knowledge to filter out artifacts which are further out. The original reconstructed picture had continuing artifacts of the same form also further away from the phantom. We note that the same was implicitly done for the Tikhonov reconstruction too since we use basis functions with support in the 128x128 square.

We move to the reconstruction of the disk phantom shown in Figure 5. We can again see a decent reconstruction result for the Tikhonov regularization, also with the same phenomenon regarding the minimum and maximum values. However, what is interesting is that the time reversal reconstruction, despite successfully localizing all the features, displays the upper right disks with lower intensity than the bottom left ones. This is in contrast with the results of the Shepp-Logan reconstruction where, despite the wrong overall scaling, all features seemed to be scaled correctly relative to each other. In practice, this might be a serious shortcoming of the time reversal method compared to the Tikhonov regularization since it also cannot be fixed by any global rescaling using some a priori information about the solution. Additionally, the bottom left disks come with significant smeared artifacts. We will see in the following section how the reconstruction quality changes when we decrease

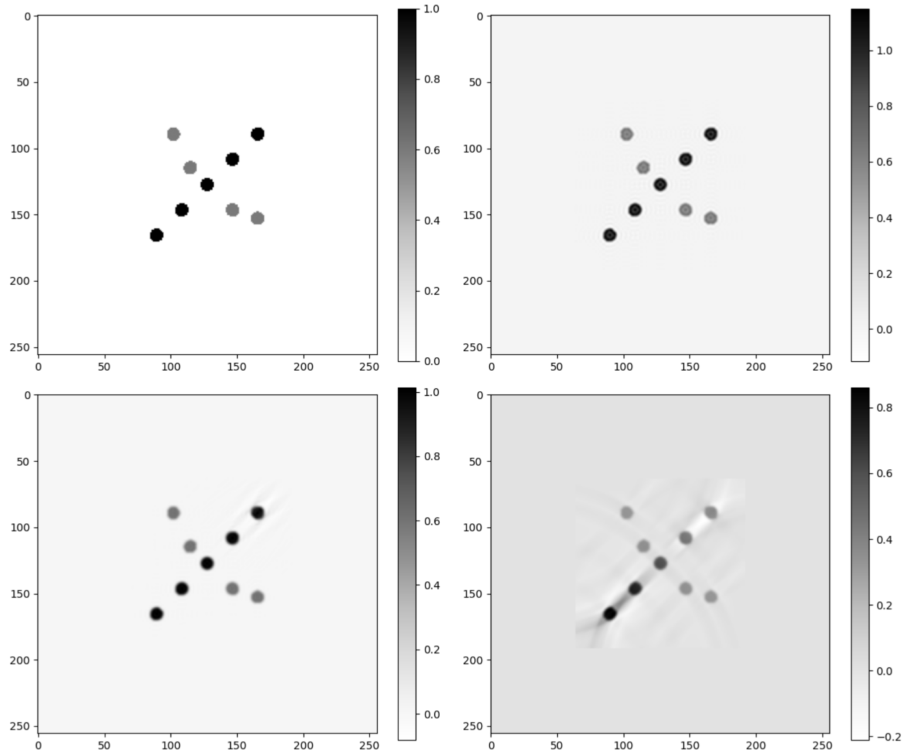

Figure 5
Reconstruction results for the disk phantom

the measurement time.

We present the relative L^2-errors for the reconstructions of both phantoms in Table 1. The first two columns show the relative errors of the two reconstructions relative to the true phantom, i.e. computed via the formula

$$relative\ error = \frac{\|true - reconstruction\|_{L^2(\Omega)}}{\|true\|_{L^2(\Omega)}}.$$

The third column displays the error made by Tikhonov reconstruction relative to the DST-projection since this should be in theory the best we can do in terms of the L^2-error. Finally, the last column displays the L^2-error of the DST-projection itself to make the composition of the total error in the second column easier to understand. With this, we can see for example that in the case of the Shepp-Logan phantom, roughly 8% error comes from the reconstruction itself while the remaining error is already present in the DST-projection.

Table 1
Relative L^2-errors

Phantom	Time reversal	Tikhonov	Tikhonov rel. to DST	DST proj.
Shepp-Logan	0.533	0.248	0.184	0.169
Disks	0.586	0.30	0.188	0.239

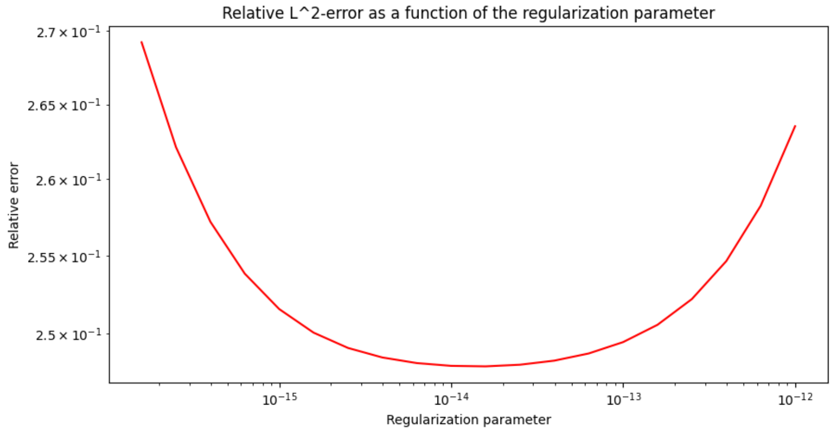

Figure 6
Relative error for the Shepp-Logan phantom reconstruction and different values of α

Before moving on to the next section, we would also like to discuss briefly the choice of the regularization parameter. We chose the value $\alpha = 10^{-14}$ as an approximate minimizer of the error curve for the Shepp-Logan phantom displayed in Figure 6. This relates nicely to the observations revolving around Equation 3. Indeed, the error curve in Figure 6 has the characteristic U-shape already predicted by the theory. For small values of α, one cannot recognize anything in the reconstruction because of the ill-conditioning of the matrix and the errors embedded in the reconstruction method like discretization error and the one caused by machine precision. For big values of α, the reconstruction is smoothed out too much and one can only recognize the rough form of the phantom and its values are of order 10^{-4}. Although the corresponding minimizer of the error curve was closer to 10^{-15} for the disk phantom, the difference was not significant and we decided to use the same value for the reconstruction of both phantoms.

3.3 Reconstruction with Insufficient Measurement Time

In this section, we aim to study the effects of shorter measurement time. First we note that the measurement time k-Wave chose is based on the diameter of the whole computational domain and is actually longer than the one necessitated by Theorem 6. In fact, we found that even for $T = 600 \cdot dt$ a reconstruction of the same quality is possible. In the case of time reversal there were no changes, while for the Tikhonov reconstruction we just needed to increase the regularization parameter to roughly $\alpha = 10^{-11}$ to obtain the same level of reconstruction quality.

A more interesting case was $T = 500 \cdot dt$. First, we present the time re-

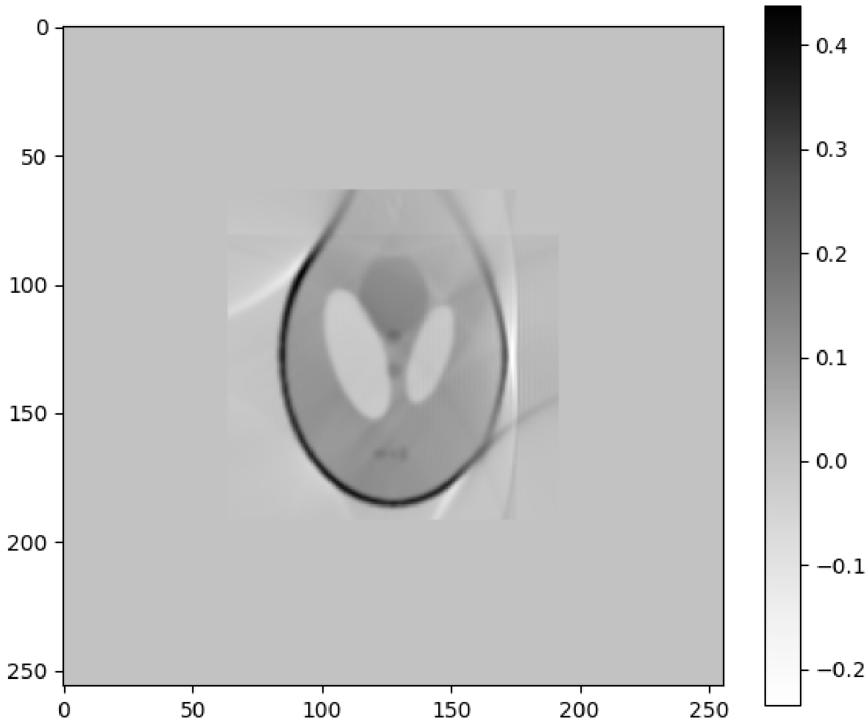

Figure 7
Time reversal for the Shepp-Logan phantom and $T = 500 \cdot dt$

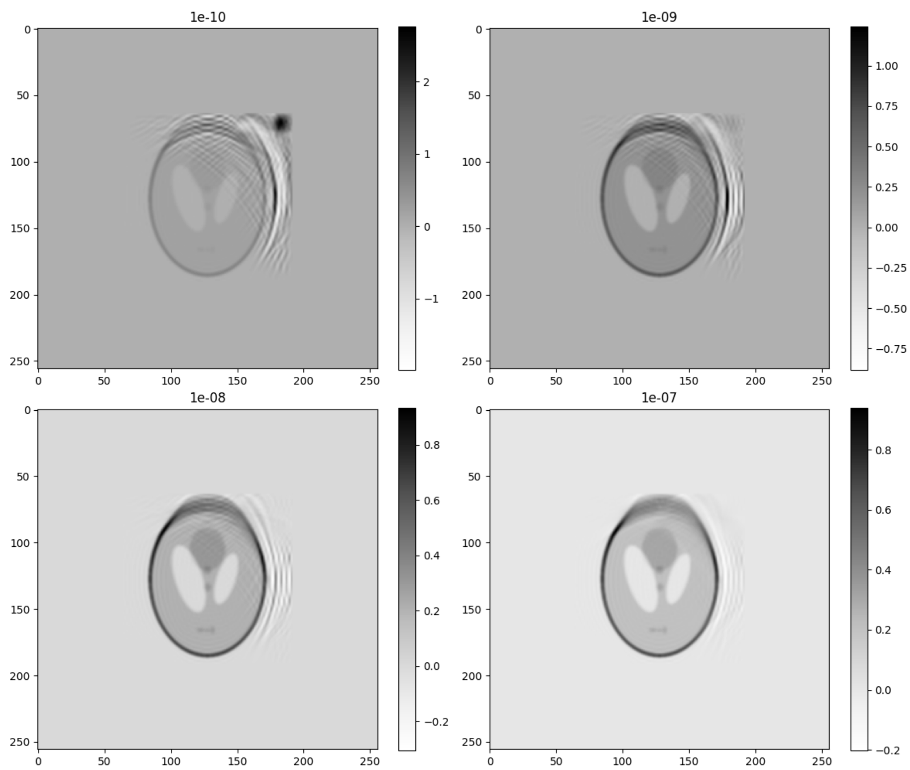

Figure 8
Tikhonov reconstruction for the Shepp-Logan phantom and $T = 500 \cdot dt$

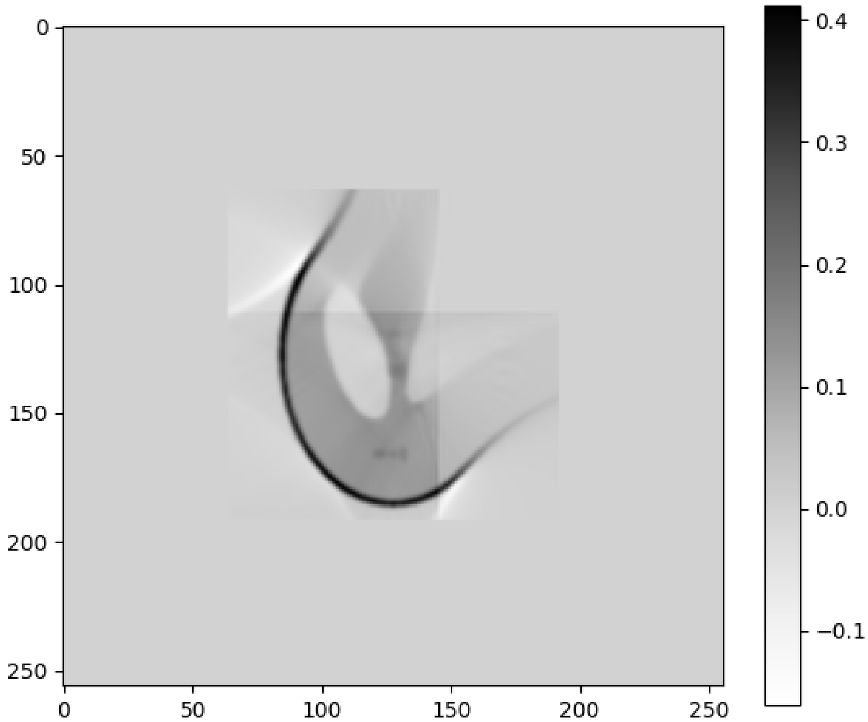

Figure 9
Time reversal for the Shepp-Logan phantom and $T = 400 \cdot dt$

versal reconstruction in Figure 7. We see that the upper edge of the phantom was not formed correctly as well as that some artifacts appeared in the right part of the picture. Last but not least, in the upper right corner of the 128x128 square we can see a small gray square seemingly containing nothing, not even any artifacts. This corresponds to the part of the 128x128 square farthest away from the detector surface. The measurement time was already too short for the signal from that part of the picture to reach the detectors. For the Tikhonov reconstruction, we first note that we had to use much bigger regularization parameters. This was caused by the linear system becoming more ill-conditioned which needed to be compensated for. We indicate the used regularization parameter above every picture in Figure 8. For $\alpha = 10^{-10}$, we get a distorted picture with a distinct black artifact in the upper right corner - the same corner which was totally invisible using time reversal. With increasing α it is filtered away together with most of the other unwanted features and the final picture with $\alpha = 10^{-7}$ offers a quite good reconstruction, although the upper edge was again not perfectly reconstructed.

For $T = 400 \cdot dt$ and $T = 300 \cdot dt$ we can see in Figures 9 and 11 the invisible square progressively increasing. Apart from that, we also see the neighboring rectangles being slightly lighter. These correspond to the parts of the picture from which the signal reaches only one part of the detector surface.

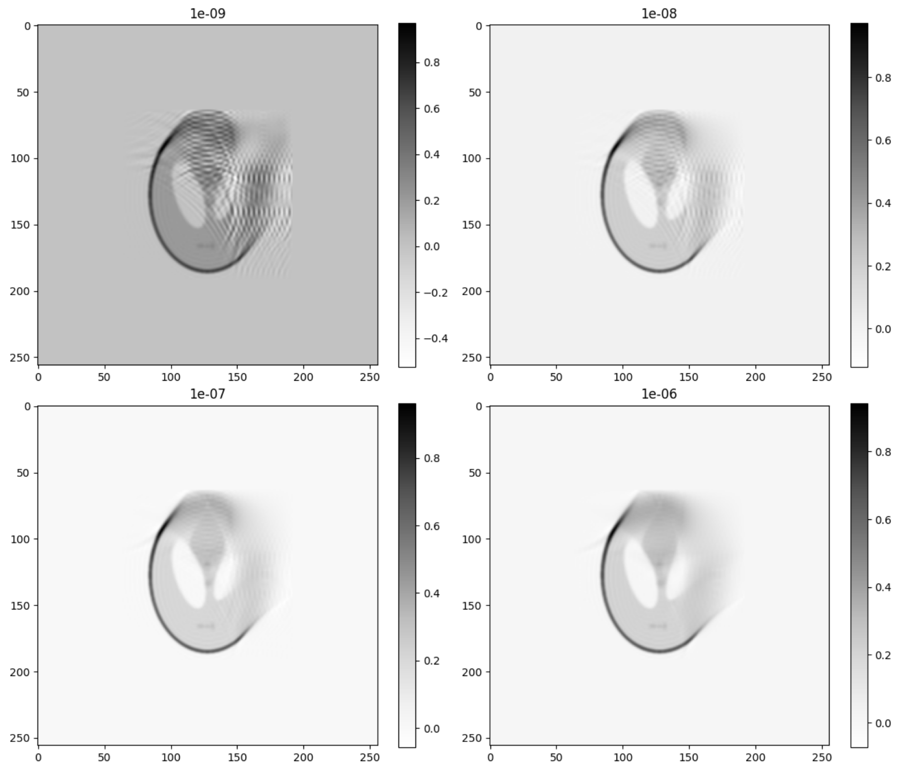

Figure 10
Tikhonov reconstruction for the Shepp-Logan phantom and $T = 400 \cdot dt$

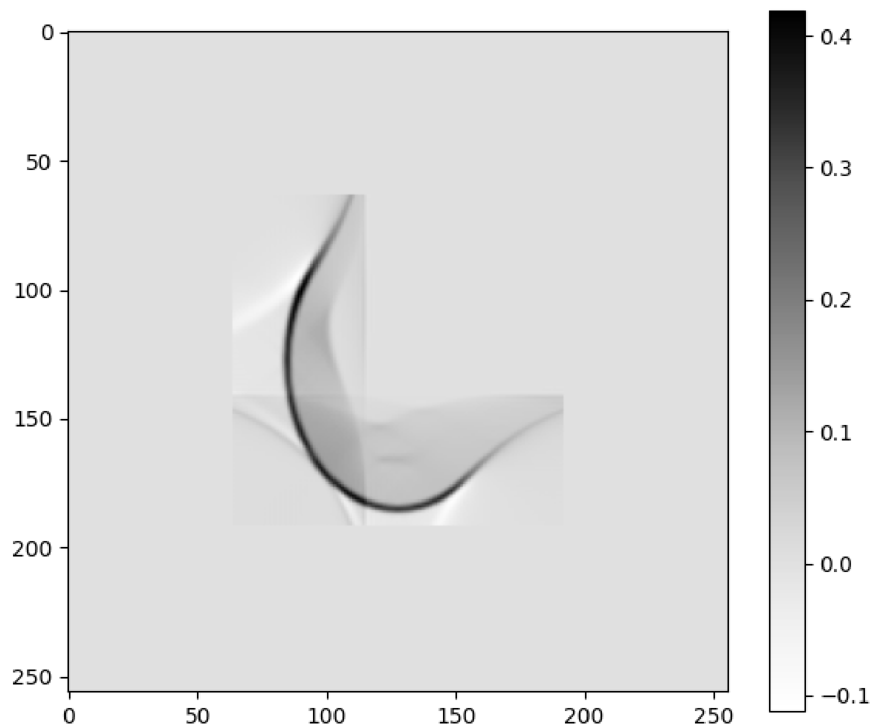

Figure 11
Time reversal for the Shepp-Logan phantom and $T = 300 \cdot dt$

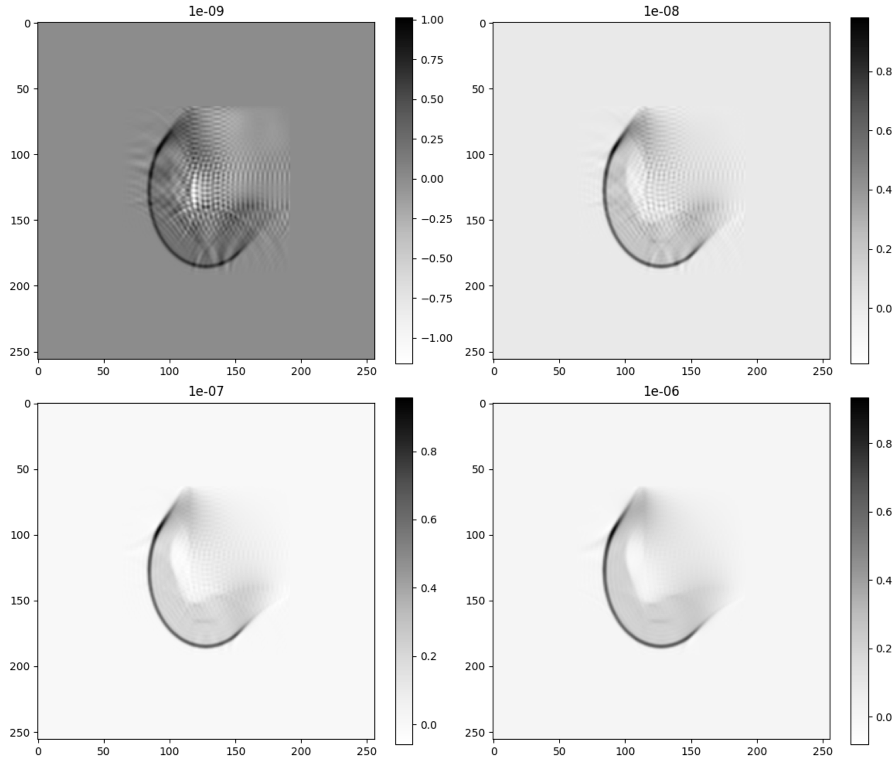

Figure 12
Tikhonov reconstruction for the Shepp-Logan phantom and $T = 300 \cdot dt$

The Tikhonov reconstruction for the same measurement times is shown in Figures 10 and 12.

Applying the same method to the disk phantom, we can see how we lose sight of one disk after another on the diagonal as the measurement time decreases and the invisibility region increases. However, the Tikhonov-based method is able to reconstruct the disks closest to the invisibility region more reliably than time reversal (as can be seen in the figures for the total measurement times $T = 500 \cdot dt$ and $T = 300 \cdot dt$). In addition to the disappearing disks, time reversal also again shows some of the recovered disks with proportionally lower intensity. That is something the Tikhonov reconstruction does not suffer from.

As before, we also present the tables containing the relative errors for both phantoms in Tables 2 and 3. We note that we again chose the regularization parameters for both phantoms based on the errors for the Shepp-Logan phantom.

Table 2
Relative L^2-errors, Shepp-Logan phantom

T	Time reversal	Tikhonov	Tikhonov rel. to DST	DST proj.
500	0.742	0.419	0.389	0.169
400	0.797	0.548	0.529	0.169
300	0.855	0.639	0.626	0.169

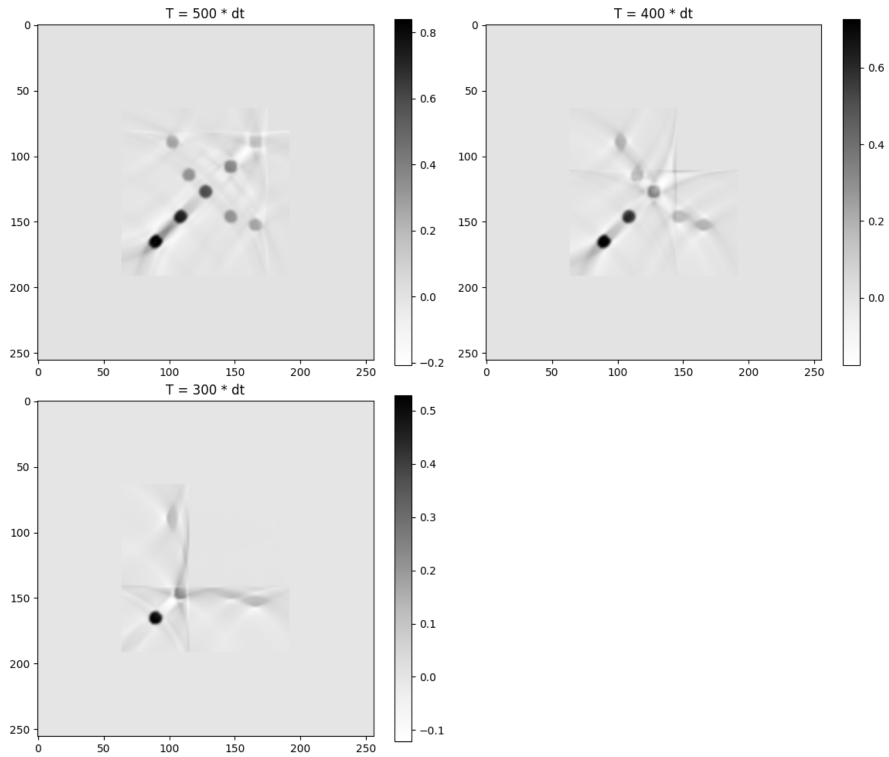

Figure 13
Time reversal for the disk phantom and different measurement times

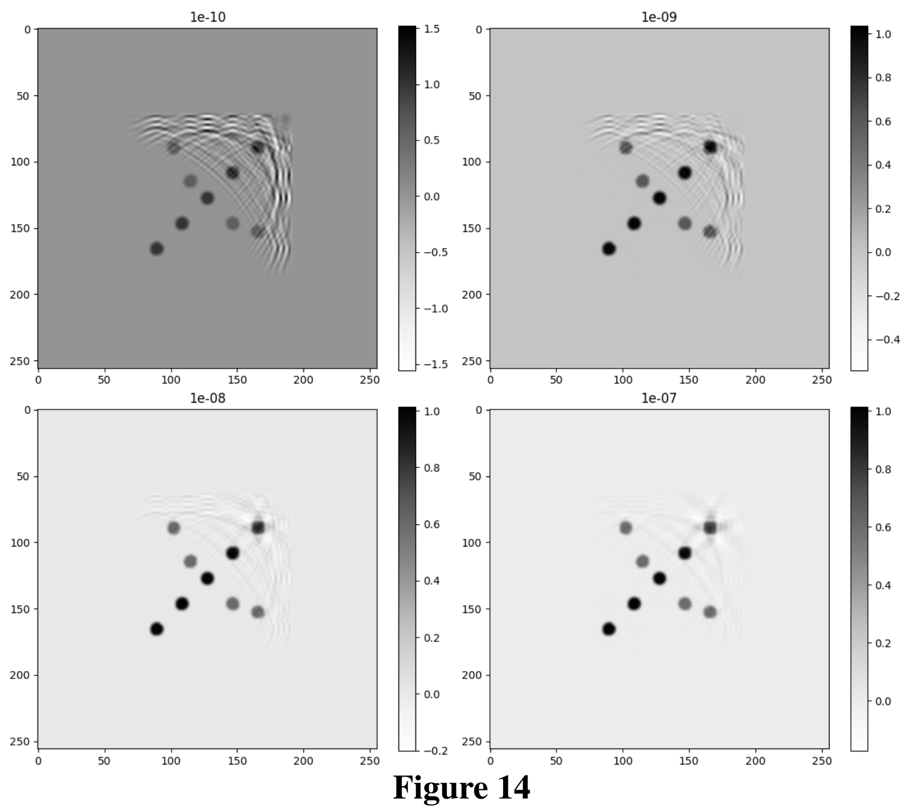

Figure 14
Tikhonov regularization for the disk phantom and $T = 500 \cdot dt$

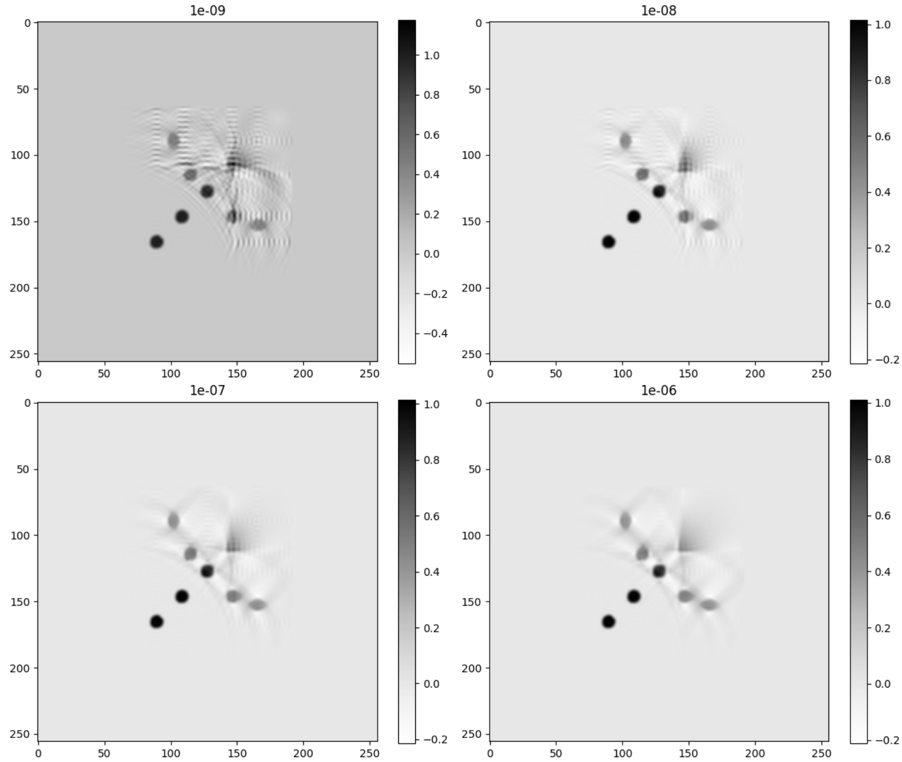

Figure 15
Tikhonov regularization for the disk phantom and $T = 400 \cdot dt$

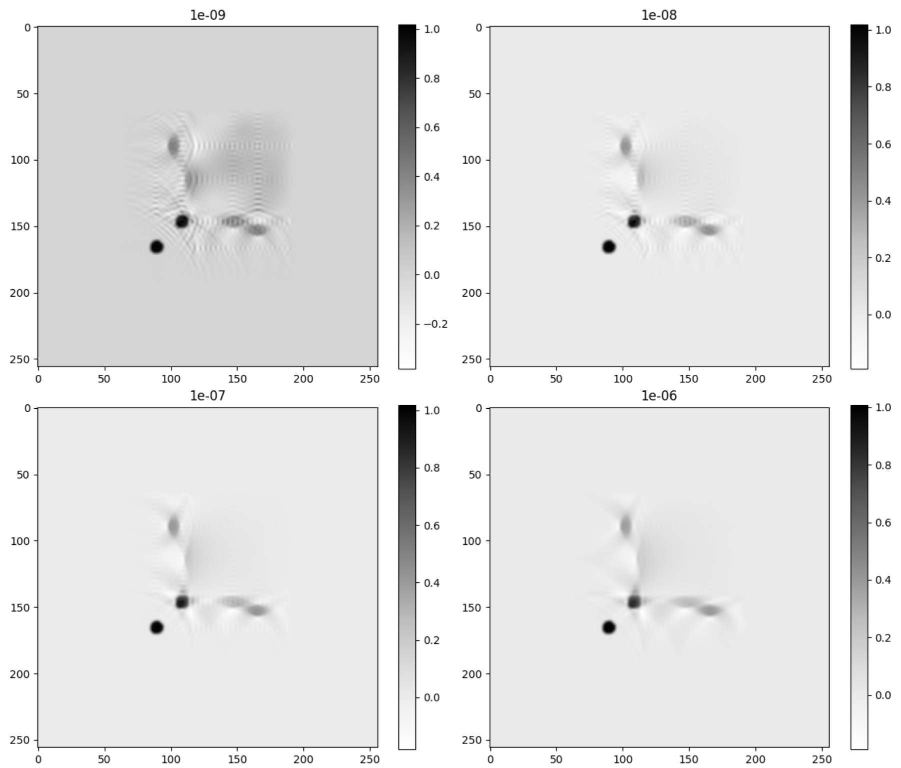

Figure 16
Tikhonov regularization for the disk phantom and $T = 300 \cdot dt$

Table 3
Relative L^2-errors, disk phantom

T	Time reversal	Tikhonov	Tikhonov rel. to DST	DST proj.
500	0.646	0.343	0.254	0.239
400	0.788	0.615	0.583	0.239
300	0.899	0.787	0.772	0.239

The Python code used to generate the results and figures in this and the preceding section can be found at https://doi.org/10.5281/zenodo.20631239.

4. Conclusion

In this thesis, we reviewed the classical theory of inverse problems and regularization. Of particular interest to us was Tikhonov regularization, which we applied to the problem of reconstructing the unique initial pressure from acoustic measurements in photoacoustic tomography. In the last chapter, we saw that this approach leads to a reconstruction method delivering good results, even when compared with the standard benchmark - the method of time reversal. In particular, our experiments using only two line detectors showed that the reconstruction method based on solving a Tikhonov-regularized system of equations seems to be less negatively affected by the limited view which such a detector setup offers than the time reversal method based on solving an underdetermined boundary value problem.

Nonetheless, the presented approach rests on a couple of somewhat unrealistic assumptions. First, the speed of sound was assumed to be constant throughout the whole domain of reconstruction, which is not the case in a realistic setting. Second, the chosen model governed by the free wave equation is not entirely accurate either. Follow-up work could therefore consist of relaxing these two assumptions: one could consider a spatially varying speed of sound and replace the free wave equation model with one also accounting for photoacoustic attenuation, e.g. as the ones studied in [4].

References

[1] Zakaria Belhachmi, Thomas Glatz, and Otmar Scherzer. A direct method for photoacoustic tomography with inhomogeneous sound speed. *Inverse Problems*, 32(4):045005, 25, 2016.

[2] Alexander Graham Bell. On the production and reproduction of sound by light. *American Journal of Science*, s3-20(118):305–324, oct 1 1880.

[3] Vladimir Britanak, Patrick C. Yip, and K. R. Rao. *Discrete Cosine and Sine Transforms: General Properties, Fast Algorithms and Integer Approximations*. Academic Press, 2007.

[4] Peter Elbau, Otmar Scherzer, and Cong Shi. Singular values of the attenuated photoacoustic imaging operator. *Journal of Differential Equations*, 263(9):5330–5376, 2017.

[5] Heinz W. Engl, Martin Hanke, and Andreas Neubauer. *Regularization of inverse problems*, volume 375 of *Mathematics and its Applications*. Kluwer Academic Publishers Group, Dordrecht, 1996.

[6] Lawrence C. Evans. *Partial differential equations*. American Mathematical Society, 2010.

[7] David Finch, Sarah K. Patch, and Rakesh. Determining a function from its mean values over a family of spheres. *SIAM J. Math. Anal.*, 35(5):1213–1240, 2004.

[8] Charles W. Groetsch. *Inverse problems in the mathematical sciences*. Vieweg Mathematics for Scientists and Engineers. Friedr. Vieweg & Sohn, Braunschweig, 1993.

[9] Per Christian Hansen. *Discrete inverse problems*, volume 7 of *Fundamentals of Algorithms*. Society for Industrial and Applied Mathematics (SIAM), Philadelphia, PA, 2010. Insight and algorithms.

[10] F. Natterer. *The mathematics of computerized tomography*. 2001.

[11] Plamen Stefanov and Gunther Uhlmann. Thermoacoustic tomography with variable sound speed. *Inverse Problems*, 25(7):075011, 2009.

[12] Bradley E. Treeby and Benjamin T. Cox. k-Wave: MATLAB toolbox for the simulation and reconstruction of photoacoustic wave fields. *Journal of Biomedical Optics*, 15(2):021314, 2010.

[13] Xueding Wang, Yongjiang Pang, Geng Ku, Xueyi Xie, George Stoica, and Lihong V Wang. Noninvasive laser-induced photoacoustic tomography for structural and functional in vivo imaging of the brain. *Nature biotechnology*, 21(7):803—806, July 2003.